International Journal of Heat and Mass Transfer 166 (2021) 120678

Contents lists available at ScienceDirect

International Journal of Heat and Mass Transfer

journal homepage: www.elsevier.com/locate/hmt

Universal Critical Heat Flux (CHF) Correlations for Cryogenic Flow Boiling in Uniformly Heated Tubes

Vishwanath Ganesan[a], Raj Patel[a], Jason Hartwig[b], Issam Mudawar[a,*]

[a] Purdue University Boiling and Two-Phase Flow Laboratory (PU-BTPFL), School of Mechanical Engineering, Purdue University, 585 Purdue Mall, West Lafayette, IN, 47907, U.S.A.
[b] NASA Glenn Research Center, Fluids and Cryogenics Branch, Cleveland, OH, 44135, U.S.A.

ARTICLE INFO

Article history:
Received 18 August 2020
Revised 8 October 2020
Accepted 31 October 2020
Available online 30 November 2020

Keywords:
critical heat flux
flow boiling
cryogens
departure from nucleate boiling, dryout
universal correlations

ABSTRACT

Experiments to determine critical heat flux (CHF) for cryogen flow in uniformly heated, round tubes have been performed throughout the globe during the past sixty years. However, experimental CHF data for cryogens are rarely published, remaining in the archives of authors, or in obscure technical reports of an organization or other inaccessible sources. In the present study, the Purdue University-Boiling and Two-Phase Flow Laboratory (PU-BTPFL) Cryogen Flow Boiling CHF Database is consolidated from world literature dating back to 1959. With 2312 data points for LH_2, LHe, LN_2 and LCH_4, it represents the largest cryogen CHF database assembled to date. The database encompasses diameters from 0.5 to 14.1 mm, critical length-to-diameter ratios from 2.5 to 230.8 (term 'critical' refers to axial location where CHF is detected), system pressures from 0.01 to 4.07 MPa, reduced pressures from 0.1 to 0.93, mass velocities from 2.2 to 8203.9 kg m^{-2} s^{-1}, inlet subcoolings from 0 to 78.9 K, inlet qualities from -2.06 to 0.95, critical subcoolings from 0 to 48.5 K, critical qualities from -1.23 to 1.00, critical void fractions from 0 to 1, and CHF values from 0.05 to 8203.9 kW m^{-2}. The consolidated database represents an invaluable tool for development of CHF correlations – a primary goal for the present study – as well as future analytic and computational models. Using this database, new universal CHF correlations are constructed for two distinct CHF mechanisms, Departure from Nucleate Boiling (DNB) and Dryout, after careful physics-based segregation of the data. With mean absolute errors below 30%, the new CHF correlations are shown to provide good predictive agreement with the database.

1. Introduction

1.1. Applications of Cryogenic Fluids

Cryogenic fluids are prevalent in numerous daily applications. For example, Liquid Nitrogen (LN_2) is used to fast freeze food, to preserve tissues and blood, and to destroy unhealthy tissues in cryosurgery. Liquid Oxygen (LOX) is used in the medical industry, life support systems, and fuel cells, while Liquid Hydrogen (LH_2) is used to cool superconducting magnets.

Cryogens, especially LOX, LH_2, Liquid Methane (LCH_4), and Liquid Helium (LHe) are also vitally important to space applications, which are the primary focus of the present study. Liquid Helium (LHe), for example, is used to chill down Earth-orbiting telescopes and satellites as well as cool space experiments. In nuclear thermal propulsion systems, LOX/LCH_4 or LOX/LH_2 are used in ascent stages, descent stages, and in-space fuel depots. LH_2 has also been proposed for use in several other advanced propulsion systems, where it may be used as both propellent and coolant. Figure 1 shows examples of the space applications of cryogens.

1.2. Fluid Physics unique to Cryogens

Cryogens constitute a unique class of fluids which are clearly distinguishable from water and refrigerants by virtue of their low saturation temperatures, as shown in Fig. 2 (calculated using REFPROP 10 [1]). But in addition to low saturation temperatures, cryogens also exhibit general thermophysical property trends, including (a) low surface tension, σ, (b) low latent heat of vaporization, h_{fg}, (c) low liquid viscosity, μ_f, and, to a lesser extent, (d) low liquid-to-vapor density difference, ρ_f - ρ_g (also calculated using REFPROP 10 [1]). These trends are clearly captured in Fig. 3, where saturated liquid property values for commonly used cryogens are plotted against reduced pressures ranging from 0 to 1 and density difference is normalized in terms of the Atwood number, *At*.

* Corresponding author: Tel. (765) 494-5705; Fax (765) 494-0539, website: .
E-mail address: mudawar@ecn.purdue.edu (I. Mudawar).
URL: https://engineering.purdue.edu/BTPFL (I. Mudawar)

https://doi.org/10.1016/j.ijheatmasstransfer.2020.120678
0017-9310/

Nomenclature

At	Atwood number, $(\rho_f - \rho_g)/(\rho_f + \rho_g)$
Bo	boiling number, $q_{CHF}/(Gh_{fg})$
Bo^*	modified boiling number, defined in Eq. (18)
C_1-C_5	empirical constants in CHF correlations
Co	confinement number, $\sqrt{\sigma/((\rho_f - \rho_g)gD^2)}$
D	inner tube diameter
f	Fanning friction factor
Fr_*	modified Froude number, $Gcos\theta/(\rho_f\sqrt{gD(\rho_f - \rho_g)/\rho_f})$
G	mass velocity
g	gravitational acceleration
h	enthalpy of fluid; heat transfer coefficient
h_{in}	inlet enthalpy of the fluid
h_{CHF}	enthalpy of fluid at CHF location
h_f	enthalpy of saturated liquid
h_{fg}	latent heat of vaporization
k_f	thermal conductivity of liquid
k_w	thermal conductivity of tube wall
L_H	heated length of tube
L_{CHF}	critical length of tube from inlet to CHF location
MAE	mean absolute error
Nu	Nusselt number
P	system pressure
ΔP	pressure drop
P_R	reduced pressure, P/P_{crit}
q	heat flux based on tube's inside area
q_{CHF}	critical heat flux (CHF) based on tube's inside area
$Re_{fo,D}$	liquid-only Reynolds number based on tube diameter, GD/μ_f
$Re_{go,D}$	vapor-only Reynolds number based on tube diameter, GD/μ_g
RMS	root mean squared error
T	temperature
T_f	bulk fluid temperature
T_{in}	bulk liquid temperature at inlet
T_{out}	bulk liquid temperature at outlet (defined only if $x_{e,out} < 0$)
T_{CHF}	local bulk liquid temperature at CHF location (defined only if $x_{e,CHF} < 0$)
T_λ	Lambda point temperature (2.17K) for Liquid Helium transitioning from LHe I to LHe II
ΔT_{sub}	liquid subcooling, $T_{sat} - T_f$
$\Delta T_{sub,in}$	inlet liquid subcooling based on pressure at inlet of heated length, $T_{sat,in}$ - T_{in}
$\Delta T_{sub,out}$	outlet liquid subcooling based on inlet temperature, energy balance for entire heated length, and pressure at outlet of heated length, $T_{sat,out} - T_{out}$
$\Delta T_{sub,CHF}$	local liquid subcooling based on inlet temperature, energy balance for entire critical length of the tube, and pressure at CHF location, $T_{sat,CHF} - T_{CHF}$
T_{sat}	saturation temperature
t_w	tube wall thickness
$We_{fo,D}$	Weber number based on tube diameter, $G^2D/(\rho_f\sigma)$
x	flow quality
x_e	thermodynamic equilibrium quality, $(h - h_f)/h_{fg}$
$x_{e,in}$	inlet thermodynamic equilibrium quality based on pressure at inlet of heated length, $(h_{in} - h_{f,in})/h_{fg,in}$
$x_{e,out}$	outlet thermodynamic equilibrium quality determined from $x_{e,in}$, energy balance for entire heated length, and pressure at outlet of heated length, $(h_{out} - h_{f,out})/h_{fg,out}$
$x_{e,CHF}$	local thermodynamic equilibrium quality determined from $x_{e,in}$, energy balance for entire critical length, and pressure at CHF location, $(h_{CHF} - h_{f,CHF})/h_{fg,CHF}$
z	axial location

Greek Symbols

α	void fraction
α_{CHF}	void fraction at CHF location
ε	height of surface roughness element
θ	percentage of data points predicted within ±30%; angle of inclination from horizontal plane
μ	dynamic viscosity
ξ	percentage of data points predicted within ±50%
ρ	density
σ	surface tension

Subscripts

A	accelerational component
CHF	critical heat flux
crit	fluid's critical point
f	liquid
F	frictional component
G	gravitational component
g	vapor
H	heated section
in	inlet of heated length
meas	measured/experimental
out	outlet of heated length
pred	predicted
sat	saturated conditions
sp	single-phase
tp	two-phase
w	tube wall

The consequence of these thermophysical property trends are reflected in the physics of both fluid flow and heat transfer for cryogens. Figure 4 shows the effects of these property trends in terms of magnitudes of three dimensionless parameters: (a) Reynolds number based on saturated liquid viscosity and tube diameter, $Re_{fo,D}$, (b) Weber number, also based on saturated liquid density and tube diameter, $We_{fo,D}$, and (c) modified Froude number, Fr_*. As shown in Fig. 4(a), very low viscosity causes cryogens to acquire much higher Reynolds numbers, especially for LHe and LH_2, compared to other fluid classes, causing cryogen flows to be predominantly turbulent and therefore enhancing single-phase liquid forced convection, albeit at the expense of higher pressure drop. Similarly, Fig. 4(b) shows how very low surface tension causes cryogens to acquire much higher Weber numbers compared to those for water and refrigerants, which causes initiation of nucleate boiling and critical heat flux (CHF) at lower wall superheats for cryogens. As to gravity effects, Fig. 4(c) shows values of modified Froude number of Fr_* greater than 6 causing fluid flow and heat transfer for cryogens to be mostly independent of flow orientation relative to Earth gravity [2]; this issue will be addressed further in a subsequent section. The three important trends captured in Fig. 4 imply correlations for cryogens are best pursued separately from those of other fluid classes.

In addition to unique fluid physics, cryogens pose appreciable challenges in experimental temperature measurements. This particularly is the case for values of wall superheat, $T_w - T_{sat}$, or wall-to-fluid temperature difference, $T_w - T_f$, approaching or below 0.5 K (which is more commonly encountered with cryogens than with water or refrigerants). In these situations, Nusselt number might exhibit erroneous trends in the form of large artificial spikes or

Fig. 1. Examples of space applications of cryogens.

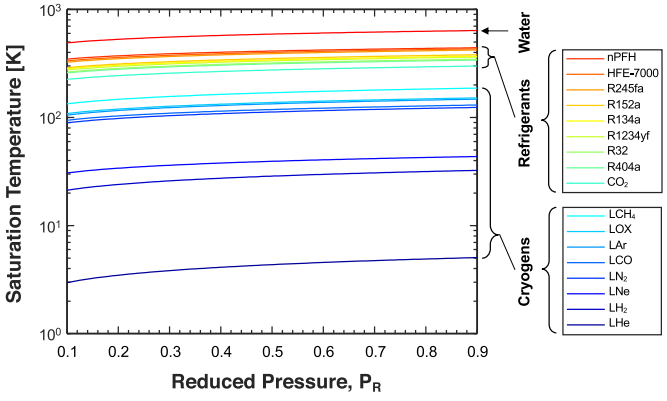

Fig. 2. Classification of coolants into water, refrigerants, and cryogens based on variation of saturation temperature with reduced pressure.

even unphysical values below zero. The rationale behind this inference can be explained as follows.

Assuming an uncertainty in wall temperature measurements of dT_w, the experimentally determined Nusselt number can be expressed as

$$Nu = \frac{hD}{k_f} = \frac{q}{T_w + dT_w - T_f}\frac{D}{k_f} = \frac{1}{1 + \frac{dT_w}{T_w - T_f}}\frac{q}{T_w - T_f}\frac{D}{k_f}. \quad (1)$$

Hence, situations where $dT_w >> (T_w - T_f)$, the calculated Nusselt number will exhibit very high measurement uncertainly, which increases with increasing dT_w and/or decreasing $T_w - T_f$. This is applicable particularly for fluids like LHe whose sub-critical operating temperatures are as low as 2.17 K (Lambda Temperature, T_λ, corresponding to transition from LHe I to LHe II).

Two important inferences regarding these temperature measurement challenges are:

(1) Investigators should always be mindful of the potential for high uncertainties when using cryogen data.
(2) These high uncertainties are certain to create appreciable scatter when aiming to develop a cryogen correlation from experimental data.

1.3. Flow Boiling Critical Heat Flux (CHF)

Critical heat flux (CHF) is arguably the most important design parameter for systems utilizing boiling to cool surfaces. This is especially the case for applications involving heat-flux-controlled heat input, where CHF can trigger a rapid unsteady rise in surface temperature, often culminating in damaging, overheating or burnout of the surface. A common design strategy is set operating conditions to achieve nucleate boiling while maintain heat flux within a safe margin below CHF. Achieving this goal requires accurate determination of CHF through all means possible, theoretical, empirical or computational.

Understanding interfacial behavior, tackling high-heat-flux removal from surfaces, and determination of CHF have been crucial cornerstones for investigations at the Purdue University Boiling and Two-phase Flow Laboratory (PU-BTPFL) dating back to the mid-1980s [3]. These efforts encompass all possible two-phase cooling schemes, including pool boiling [4-7], falling films [8-10], macro-channel flow boiling [11-14], mini/micro-channel flow boiling [15,16], jet impingement [17,18] and spray cooling [19,20]. The

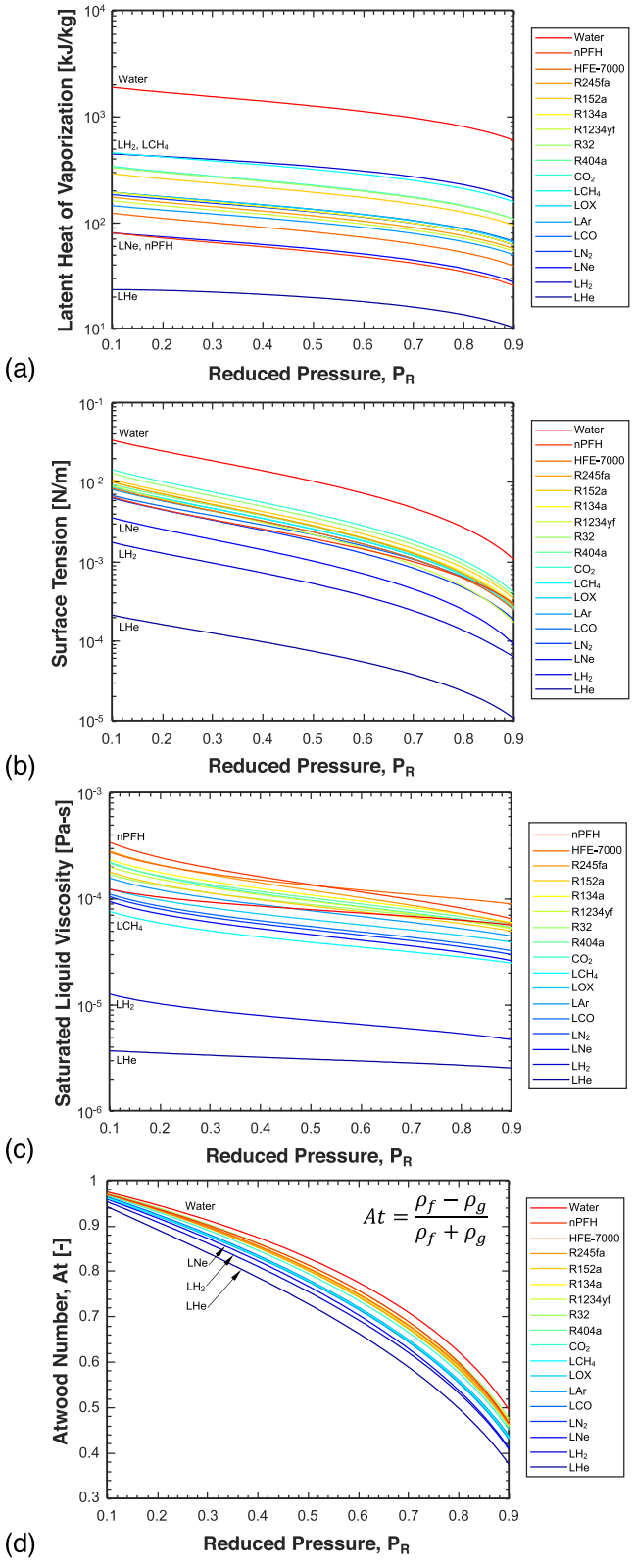

Fig. 3. Variations of (a) latent heat of vaporization, (b) surface tension, (c) saturated liquid viscosity, and (d) Atwood number with reduced pressure for cryogens compared to those of other fluid classes.

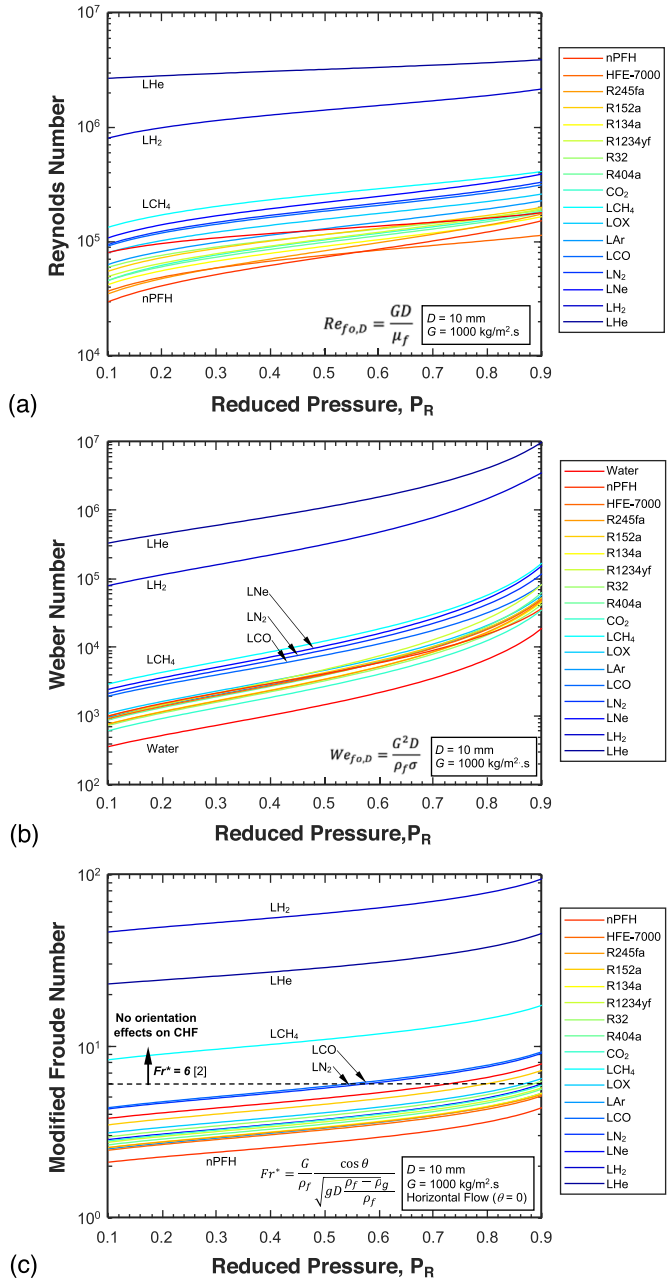

Fig. 4. Variations of (a) Reynolds number, (b) Weber number, and (c) modified Froude number (also Hall and Mudawar's [2] criterion for neglecting orientation effects) with reduced pressure for cryogens along with those of other fluid classes for $D = 10$ mm and $G = 1000$ kg/m^2.s.

reader is advised to refer to the interfacial physics interpretations provided in these studies, especially in regard to CHF determination.

For flow boiling in tubes two main types of CHF are commonly encountered: Dryout and Departure from Nucleate Boiling (DNB) [21]. As shown in Fig. 5, Dryout is typically encountered in channels where the coolant is supplied with low subcooling and at low mass velocity and subjected to low wall heat flux. Assuming the channel in sufficiently long, these conditions lead to a gradual increase in vapor void fraction along the channel, encompassing bubbly, slug and annular flow regimes. Here, CHF is associated with eventual dryout of the annular liquid film. Because of the combination of low wall heat flux and axial conduction in the wall, Dryout is comparatively a mild form of CHF. Owing to low latent heat

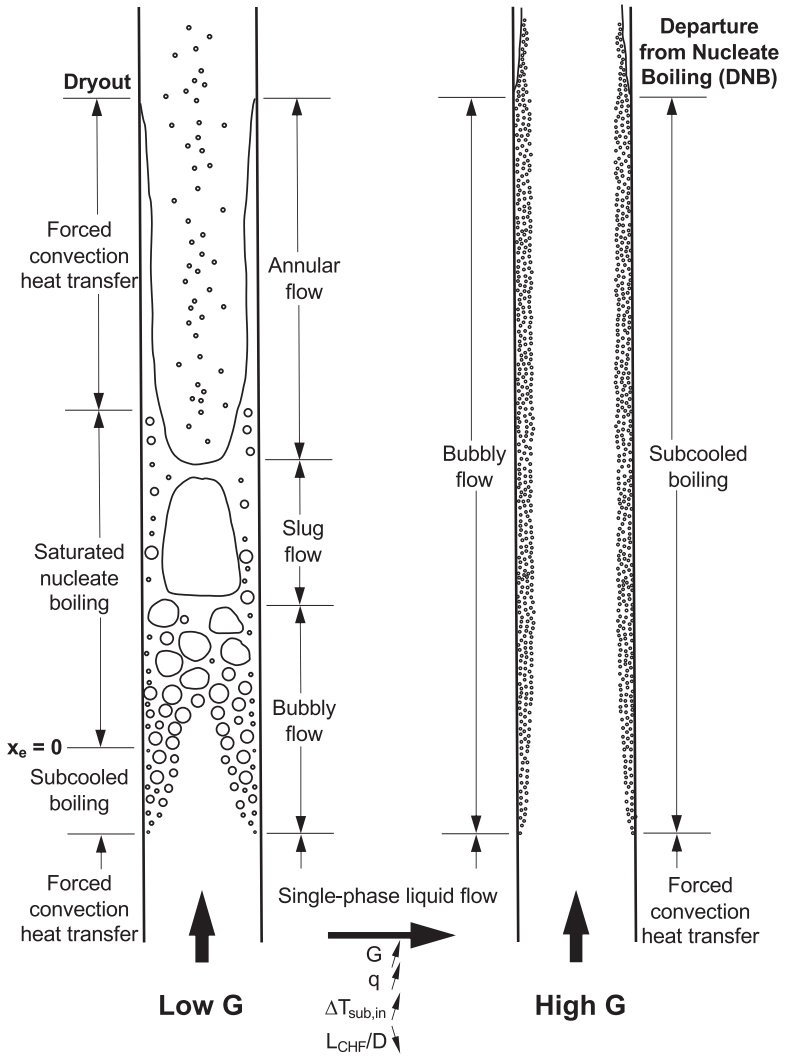

Fig. 5. Heat transfer flow patterns associated with flow conditions leading to CHF due to Dryout and Departure from Nucleate Boiling (DNB) in a uniformly heated tube. Adapted from Mudawar and Bowers [21].

of vaporization and low surface tension, the nucleate boiling region for cryogens ends up occupying a comparatively smaller fraction of the entire heated length compared to water and refrigerants. It is for the same reasons that much higher exit qualities are achieved with cryogens.

On the other hand, DNB, which is also depicted in Fig. 5, is generally encountered when the coolant is supplied to the channel in highly subcooled state and at high mass velocity and is subjected to high wall heat flux. Here, bubbles are unable to penetrate towards the liquid because of strong condensation effects in the core. CHF is triggered along the wall because of localized coalescence of vapor bubbles into an oblong vapor blanket, even at axial locations with abundant liquid flow in the core. The vapor blanket serves to preclude liquid access from the core to the wall and, because of high wall heat flux, cause the wall temperature to escalate in a rapid unsteady fashion. This is why DNB is often associated with high probability of physical damage to the heating wall compared to Dryout. However, it can be argued that since cryogens, unlike other fluid classes, are associated with relatively low heat fluxes, as well as low CHF values, physical burnout is unlikely with cryogens.

Figure 5 clearly shows how CHF in both its forms is influenced by the coolant's mass velocity, G, inlet subcooling, $\Delta T_{sub,in}$, tube diameter, D, and heated length, L_H, in addition of course to the coolant's thermophysical properties, which in turn are dictated by operating pressure, P. Different functional forms have been recommended to correlate CHF data [22]. The first involves relating CHF to local (or outlet) conditions where CHF is encountered,

$$q_{CHF} = f(D, G, P, h_{CHF}). \tag{2}$$

Another is based on inlet conditions and axial location for CHF occurrence, L_{CHF},

$$q_{CHF} = f(D, L_{CHF}, G, P, h_{in}). \tag{3}$$

Yet, a third form, similar to the second except that CHF is assumed to occur at the exit of the heated length (*i.e.*, $L_{CHF} = L_H$) is,

$$q_{CHF} = f(D, L_H, G, P, h_{in}). \tag{4}$$

In nondimensional form, Eqs. (2) and (3) can be written, respectively, as [22]

$$Bo = \frac{q_{CHF}}{Gh_{fg}} = f\left(We_{fo,D}, \frac{\rho_f}{\rho_g}, x_{e,CHF}\right). \tag{5}$$

$$Bo = \frac{q_{CHF}}{Gh_{fg}} = f\left(We_{fo,D}, \frac{\rho_f}{\rho_g}, x_{e,in}, \frac{L_{CHF}}{D}\right). \tag{6}$$

Most of the seminal correlations reported in the literature (see Hall and Mudawar [22] and Katto and Ohno [23]) do obey the

functional forms of Eqs. (5) and (6). On close inspection, it can be seen that CHF correlation generally exhibit dependence on Weber number, either density ratio or reduced pressure (which also dictates thermophysical property values for saturated liquid and saturated vapor), and either outlet quality (or outlet subcooling) or a combination of inlet quality (or inlet subcooling) and tube geometry.

Since the flow physics and CHF mechanism are fundamentally different for the two CHF types, it imperative to make a distinction between them when using any data to develop a CHF correlation. This notion will be carefully addressed in a subsequent section.

1.4. Flow Boiling CHF in Cryogenic Fluids

There is presently a pressing need to acquire accurate predictive tools for cryogen two-phase flow and heat transfer in tubes in many of the aforementioned space applications. Prevalence of two-phase flow in these applications can be easily explained using LH_2 as example. Used both as propellent and coolant, low boiling point LH_2 is stored in liquid state but must be transferred to a variety of systems in gaseous form. This implies the LH_2 will undergo flow boiling during the transfer process.

The importance of acquiring accurate predictive tools for cryogens is evident from concerted efforts by the National Aeronautics and Space Administration (NASA) (also the National Institute of Standards and Technology (NIST)) involving use of cryogens for a variety of applications, with conditions ranging from sub-critical to super-critical, and from pool boiling (nucleate boiling heat transfer coefficient and CHF) to flow boiling (two-phase pressure drop, two-phase heat transfer coefficient, and CHF [24,25]).

Overall, fluid class has a very strong influence on magnitude of CHF in flow boiling situations. For water, measured CHF values range from $\sim$ 1 to over 200 MW/m^2 [20]. On the other hand, CHF for refrigerants, especially for applications involving thermal management of electronic devices in such applications as supercomputers, hybrid vehicle power electronics and both commercial and military avionics, ranges from $\sim$ 1 to 10 MW/m^2 [2]. However, cryogenic fluids, which exist in liquid state at extremely low temperatures, because of their weak thermophysical properties (as shown earlier in Fig. 3), exhibit comparatively much lower CHF values. Examples include (as will be discussed later in the present study) $\sim$10 kW/m^2 for LHe, $\sim$100 kW/m^2 for LH_2, $\sim$100 – 1000 kW/m^2 for LN_2, and $\sim$1 MW/m^2 for LCH_4. These low CHF values limit the application of cryogens to a unique set of applications.

For both water and refrigerants, a primary focus of experimental studies is to distinguish the mechanism for CHF (Dryout versus DNB) as well as obtain quantitative measurements of interfacial behavior at conditions just preceding CHF occurrence. Aside from heat transfer measurements, flow visualization plays a vital role is terms of capturing dominant flow patterns and clearly distinguishing DNB type CHF from Dryout. Unfortunately, flow visualization in cryogenic experiments is extremely limited, rendering any systematic confirmation of CHF type quite elusive. However, a few exceptions do exist, where flow visualization is conducted concurrently with the heat transfer measurements to aid in determination of CHF type.

The mechanism of DNB in associated with several interrelated processes, including detailed evolution of the two-phase flow along the channel, initial formation of localized vapor blankets, and most importantly, hydrodynamic instability (Helmholtz type) governing when the interface of the vapor blanket switches from unstable state (condition allowing bulk liquid to contact the heated wall and therefore avoid DNB) to stable state (condition where liquid is no longer able to access the heated wall, therefore resulting in CHF). These concepts are fairly well known from prior works by one of the authors and widely disseminated in the heat transfer literature since the early 1990s (see ref. [14]) and therefore not elaborated upon here. However, it is obvious that every aspect of the two-phase flow that culminates in DNB is dependent on the fluid's thermophysical properties, which is captured in relevant dimensionless groups. Therefore, while the DNB mechanism might be similar for different fluid types, both the DNB trends and details are quite different. This is especially the case for cryogens, given their property values deviate markedly from those of other fluid types.

Predicting two-phase flow and heat transfer for cryogens can be achieved using (a) experimental correlations, (b) analytic models, and (c) CFD models. While PU-BTPFL investigators have successfully developed both analytic models [26–29] and CFD models [30,31] for both flow boiling and flow condensation (these are all specific to thermal management of space systems), these efforts required very systematic and exhaustive validation using a variety of flow visualization and flow measurement techniques, which are extremely limited for cryogens, especially in terms of determining CHF type. This leaves experimental correlations as the primary rational means for predicting two-phase transport behavior for cryogens.

Developing reliable correlations requires first amassing available databases for different cryogens into a single, unified database – this represents the first primary goal of the present study in terms of CHF prediction. A key question in pursuing this goal is determine whether to employ 'universal correlations' for all fluid types (water, refrigerants and cryogens) or cryogens alone. Developing universal correlations has been the target of several recent efforts at PU-BTPFL based on massive databases for all fluid types and very broad ranges of key operating conditions, such as pressure, mass velocity, quality, and tube geometry (e.g., [32]). The difficulty in adopting the same methodology for cryogens is large bias in terms of high data count for both water and refrigerants compared a relatively small count for cryogens. This implies that, even when a universal correlation does achieve good overall accuracy in predicting data for all three fluid classes, predictive accuracy might be compromised for fluids with low data count. This implies a better strategy might be to pursue three separate universal correlations, one for water, one for refrigerants, and one for cryogens. Developing a universal CHF correlation for cryogens represents the second primary goal of the present study.

But even when aiming to develop a universal CHF correlation using a large database for multiple cryogens, it is of paramount importance to first demarcate data based on three primary classifiers: (1) fluid, (2) CHF mechanism (Dryout versus DNB), and (3) flow orientation in order to assess major data trends associated with each classifier. This strategy will be systematically adopted in the present study before developing a universal correlation applicable to the entire database.

1.5. Objectives of Present Study

The present study is motivated by the lack of a large, reliable, error-free cryogen CHF database for developing correlations and mechanistic models to predict CHF in flow boiling. Another motivation was the lack of a simple, accurate, universal CHF correlation for cryogenic flow in a uniformly heated tube.

Following are key objectives of the present study:

(1) Amass cryogenic fluid flow boiling CHF databases available from the world literature for uniformly heated tubes.
(2) Carefully assess the accumulated data on a point-by-point basis to exclude for any inaccurate data or data or missing vital information such as operating conditions and apply systematic criteria for data exclusion.

(3) Compile a new PU-BTPFL Cryogen CHF Database free from aforementioned exclusions.
(4) Carefully segregate the compiled data based on fluid (LH_2, LHe, LN_2, and LCH_4), flow orientation (vertical upflow, downflow or horizontal flow), and CHF mechanism (Dryout or DNB).
(5) Using the CHF Database, develop new 'Universal CHF Correlations' for cryogens.
(6) Using the CHF Database, test the performance of existing CHF correlations.
(7) Ascertain the accuracy of the new correlation for each fluid and against each primary variable (mass velocity, system pressure or reduced pressure, diameter, and critical quality).
(8) Identify 'gaps' in the available CHF data which warrant further experimental investigation.
(9) Recommend a methodology for acquiring future CHF data in a manner that is conducive to refining CHF correlations and mechanistic models.

2. Compilation of Cryogen Flow Boiling CHF Database

As indicated earlier, the present study involved exhaustive data mining of Flow Boiling cryogen CHF data from all literature sources available to the present authors. This included (1) major cryogen journals (*e.g.,* Cryogenics (Elsevier), Advances in Cryogenic Engineering (Springer), (2) major cryogen conferences (e.g., International Cryogenic Engineering Conference, Cryogenic Engineering Conference (early papers published in Advances in Cryogenic Engineering)), (3) NASA and NIST technical reports, and (4) other sporadic publications, reports and theses from across the globe.

Unless CHF data was explicitly specified in a given reference, the database was amassed by finding CHF information using one of three methods: (1) extracting maximum nucleate boiling heat flux data from boiling curves, (2) locating the point of wall temperature excursion from wall temperature versus heat flux plots, and (3) locating the point of heat transfer coefficient deterioration from heat transfer coefficient versus heat flux plots.

The data mining effort was complicated by difficulty acquiring certain references because of such factors as (a) lack of availability from international interlibrary services, (b) reluctance of a few investigators to share their own database, and (c) duplicate data. Avoidance of duplicate data was a thorough and time-consuming effort, necessitated by the fact that many published works lacked clear indication of sources for the data presented. Overall, the possibility of data duplication in the CHF database was prevented by careful point-by-point inspection of the acquired data.

After completing the initial data mining effort and making certain of absence of duplicate data, efforts shifted to excluding data that did not strictly conform to the following uniformity requirements:

(1) Only single-component cryogens, therefore excluding data for binary or higher order mixtures.
(2) Flow in only straight circular tubes; data for non-circular test sections (*e.g.,* rectangular, square, annular, rod, bundle) or helical tubes are excluded.
(3) Flow in only stationary tubes; data for rotating tubes are excluded.
(4) Flow not involving use of swirl flow promotor (*e.g.,* twisted tape insert) within the tube or upstream of the tube's inlet.
(5) Flow not involving use of abnormal test section inlet or outlet (*e.g.,* orifice plate, inlet expansion, outlet expansion).
(6) Flow in tubes whose inner walls are not modified (*e.g.,* finned) for the purpose of enhancing heat transfer performance.
(7) Only data for vertical upflow, vertical downflow, and horizontal flow; data for inclines tubes are excluded.
(8) Only uniformly heated circular tubes; data for axially or circumferentially nonuniform wall heat flux are excluded.
(9) CHF data obtained from quenching experiments, which are prone to appreciable measurement error due mostly to fast temperature transients, are excluded.
(10) Only CHF data presented by original authors with documented values for every parameter necessary for correlating the data (*e.g.,* operating pressure, mass velocity, inlet or outlet subcooling, tube geometry, heat flux, *etc.*).

This exclusion strategy, summarized in Table 1, resulted in an initial database suitable for developing correlations (also future models) for the complex CHF phenomenon specific to cryogens. However, it is important to note that the above do not constitute a complete list for data exclusion as other considerations, discussed in a later section, preclude inclusion of certain additional datapoint. These constitute additional fundamental exclusions, achieved through further assessment of the amassed data, in pursuit of the final PU-BTPFL Cryogen Flow Boiling CHF Database.

3. Assessment of World CHF Data

3.1. Experimental Methods used by Prior Investigators

3.1.1. Wall material, thickness and roughness

Test section material, wall thickness, surface roughness, and surface aging are all the effects that may influence flow boiling heat transfer and CHF. Tube material information and to a lesser extent wall thickness are mentioned in most references covered in the current study. Unfortunately, surface roughness is rarely described in research publications. Exceptions of studies that do provide ample description of surface roughness are those by Zhang *et al.* [64], Steiner and Schlünder [67], Müller [93], and Hilderbrandt [56].

Because of overall lack of complete information in many of the references on wall related issues, especially surface roughness and surface aging, a thorough investigation of these on CHF for cryogens is not possible at the present time.

3.1.2. Pressure measurement and pressure drop considerations

The majority of the studies were found to lack mention of whether the reported system pressure is the measured inlet or outlet pressure, perhaps because of relatively large diameter of tube tested and therefore negligible pressure drop. Only Van Noord [97] provided both inlet and outlet pressure information.

Fortunately, some authors do provide pressure drop data as well. It is found for most studies that provided pressure drop data that maximum pressure drop along the tube is quite small, which allows use of constant pressure assumption as suggested by Katto and Yokoya [98] using the criterion $\Delta P_{max}/P < 0.1$, where P is the quoted system pressure. This, and absence of mention whether quoted system pressure was measured at inlet or exit, justifies using system pressure alone (*i.e.,* assuming constant pressure) as basis for determining values for saturated thermophysical properties when correlating CHF data. This approach is used throughout the present correlation effort, where either inlet or outlet pressures are provided.

To systematically verify this assumption of constant pressure, the present authors employed a conservative (high) estimate for ΔP_{max} between the inlet and axial location where CHF was reported to occur. For axial locations where $x_e < 0$, the portion of pressure drop associated with single-phase liquid is calculated using Colebrook's friction factor relation [99], with any applicable gravitational pressure drop included as well,

Table 1
Exclusion strategy for cryogen flow boiling CHF data in uniformly heated straight tubes.

Reference	Deviations from standard configuration [a]	Data points missing values for crucial parameters	Presence of duplicate data	Excluded due to other factors	Remarks
(a) Complete Exclusion					
Dean & Thompson [33]	•				Annular circular test section with heater in the core
Walters [34]		•			Only overall range for mass velocity provided
Lehongre *et al.* [35]		•			Inlet quality information missing
Jergel & Stevenson [36]	•				Rectangular channel test section with only a small fraction of test section heated
Jergel *et al.* [37]	•				Rectangular channel test section with only a small fraction of test section heated
Jergel & Hlasnik [38]	•				Rectangular channel test section with only a small fraction of test section heated
Grigoriev *et al.* [39]			•		Current data with additional new data found in Grigoriev *et al.* [54]
Subbotin *et al.* [40]		•			Inlet quality information missing
Lu [41]	•				Rectangular channel test section with discrete heat sources
Klimenko *et al.* [42]		•			Only overall ranges for mass velocity, pressure and quality provided
Klimenko & Sudarchikov [43]		•			Only overall range for pressure provided and inlet quality information missing
Qi *et al.* [44]		•			Only overall range for inlet quality provided
Qi *et al.* [45]		•			Only overall ranges for pressure and inlet quality provided
Trejo *et al.* [46]	•				Square and rectangular channel test sections
Mustafi [47]	•				Dry-out occurring in helically shaped pre-heater
Shiotsu *et al.* [48]	•				Annular circular test section with heater in the core
Tatsumoto *et al.* [49]	•				Annular circular test section with heater in the core
Yoneda *et al.* [50]	•				Rectangular duct test section with single-sided heating
Matsumoto *et al.* [51]	•				Annular circular test section with heater in the core
Shirai *et al.* [52]	•				Annular circular test section with heater in the core
An *et al.* [53]		•			Pressure and inlet quality information missing
(b) Partial Exclusion[b]					
Lewis *et al.* [55]		•			Inlet quality information missing for certain data points
Hilderbrandt [56]		•			Only overall ranges for mass velocity and pressure provided for certain data points
Ogata & Sato [57]				•	Certain data points difficult to extract due to similarity in symbols used
Ogata & Sato [58]		•			Only overall ranges for pressure and mass velocity provided for certain data points
Petukhov *et al.* [59]		•			Only overall ranges for mass velocity and inlet quality provided for certain data points
Petukhov *et al.* [60]	•				Certain tests performed using rotating test section
Yun *et al.* [61]	•				Certain tests performed using circular test section with wire coil inserts
Zhang & Fu [62]		•			Wall temperature not provided to extract CHF data from certain heat transfer coefficient data points
Zhang *et al.* [63]		•			Only overall range for pressure provided for certain data points
Zhang *et al.* [64]		•			Only overall range for pressure provided for certain data points and inlet quality information missing for certain data points

[a] Standard flow conforming to all requirements stated in section 2.
[b] Select data points are excluded while are deemed acceptable for inclusion in final CHF Database.

$$\frac{dP_{sp,f,F}}{dz} = \frac{2}{D} f_{sp,f} \frac{G^2}{\rho_f}, \tag{7}$$

$$\frac{1}{\sqrt{4f_{sp,f}}} = -2\log_{10}\left(\frac{\varepsilon}{3.7D} + \frac{2.51}{Re_{fo,D}\sqrt{4f_{sp,f}}}\right), \tag{8}$$

$$\text{and } \frac{dP_{sp,f,G}}{dz} = \rho_f g sin\theta. \tag{9}$$

Whereas, for the axial locations where $x_e \geq 0$, pressure drop includes frictional, accelerational and gravitational components. The accelerational and gravitational gradients are determined, respectively, according to

$$-\frac{dP_{tp,A}}{dz} = G^2 \frac{d}{dz}\left\{\frac{x_e^2}{\alpha\rho_g} + \frac{(1-x_e)^2}{(1-\alpha)\rho_f}\right\}, \tag{10}$$

$$\text{and } -\frac{dP_{tp,G}}{dz} = \left(\alpha\rho_g + (1-\alpha)\rho_f\right) g sin\theta, \tag{11}$$

where the void fraction α is calculated using Zivi's [100] relation

$$\alpha = \left[1 + \left(\frac{1-x_e}{x_e}\right)\left(\frac{\rho_g}{\rho_f}\right)^{2/3}\right]^{-1}. \tag{12}$$

Finally, total pressure drop ΔP is determined by integrating the pressure gradient relations for single-phase and two-phase region over the respective axial span for each. Notice that, for the two-phase region, frictional pressure gradient is bound on the lower side by that for pure saturated liquid and on the upper side pure saturated vapor, both calculated using Colebrook's friction factor relation [99], *i.e.,*

$$0 \leq \frac{\Delta P_{tp,F} - \Delta P_{sp,f,F}}{\Delta P_{sp,g,F} - \Delta P_{sp,f,F}} \leq 1. \tag{13}$$

Therefore, a conservative high estimate for total pressure drop, ΔP_{max}, is found by replacing the two-phase frictional pressure drop for axial locations where $x_e > 0$ by that corresponding to single-phase saturated vapor.

$$\frac{dP_{sp,g,F}}{dz} = \frac{2}{D} f_{sp,g} \frac{G^2}{\rho_g}, \tag{14}$$

$$\text{and } \frac{1}{\sqrt{4f_{sp,g}}} = -2\log_{10}\left(\frac{\varepsilon}{3.7D} + \frac{2.51}{Re_{go,D}\sqrt{4f_{sp,g}}}\right). \tag{15}$$

Owing to the conservative nature of the maximum pressure drop (which definitely exceeds the actual pressure drop), the constant pressure assumption as suggested by Katto and Yokoya [98] is slightly relaxed to $\Delta P_{max}/P < 0.2$. A key advantage of this method is lack of reliance on the myriad of possible models or correlations for calculating the two-phase frictional pressure gradient.

Overall, the criterion $\Delta P_{max}/P < 0.2$ is valid for almost all cases, excepting a few data points by Grigoriev *et al.* [54], Shirai *et al.* [65], and Wright and Walters [66], where $\Delta P_{max}/P > 0.2$, which are excluded from the CHF database. Table 2 provides more details on

Table 2
Summary of data points excluded from the CHF database for violating constant pressure assumption.

Reference	Total CHF data points	High $\Delta P_{max}/P$[a] Low *Co*	High $\Delta P_{max}/P$[b] High *Co*	ΔP_{max} out of bounds[c]	Acceptable CHF data points
Liquid Hydrogen					
(a) Vertical Upflow					
Shirai *et al.* [65]	381	1			380
(b) Horizontal Flow					
Wright and Walters[d] [66]	2	1			1
Liquid Nitrogen					
(a) Vertical Upflow					
Grigoriev *et al.* [54]	23	2	3	11	7
Shirai *et al.* [65]	122	1			121
		5	**3**	**11**	

[a] Data with $\Delta P_{max}/P > 0.2$ and $Co \leq 1.5$
[b] Data with $\Delta P_{max}/P > 0.2$ and $Co > 1.5$
[c] High *Co* data (> 1.5 and in some cases > 3) with high pressure drop causing pressure to go out of bounds for evaluation of thermophysical properties in REFPROP 10 [1]
[d] Data extracted from Steiner and Schlünder [67]

data points violating the constant pressure assumption and therefore excluded from the CHF database.

3.2. Energy Balance Verification

The first law of thermodynamics requires that the energy content of a unit mass of fluid at any axial location along the tube (local enthalpy) equals the energy content at the inlet (inlet enthalpy) plus the heat supplied from the tube wall from the inlet to the same axial location. For the axial location L_{CHF} where CHF occurs, the energy balance can be written as

$$h_{CHF} = h_{in} + 4\frac{L_{CHF}}{D}\frac{q_{CHF}}{G}. \tag{16}$$

By employing the aforementioned constant pressure assumption, Eq. (16) can be re-written as

$$x_{e,CHF} = x_{e,in} + 4Bo\frac{L_{CHF}}{D}. \tag{17}$$

It is important to note here that $x_{e,CHF}$ is not necessarily equal to the exit quality since L_{CHF} is not always equal to the total heated tube length L_H.

By carefully examining the available data sources for cryogens, it was observed that CHF data were presented in individual studies in one of four kinds: (a) data having both inlet quality, $x_{e,in}$, and critical thermodynamic equilibrium quality, $x_{e,CHF}$, (b) data with only inlet thermodynamic equilibrium quality, $x_{e,in}$, along with either entire heated length, L_H, where CHF occurs at the outlet, or critical length, L_{CHF}, (c) data with only critical thermodynamic equilibrium quality, $x_{e,CHF}$, along with axial location of CHF, L_{CHF}, and (d) data with only critical thermodynamic equilibrium quality, $x_{e,CHF}$, along with the entire heated length, L_H, and thermodynamic equilibrium quality operational range ($x_{e,min} - x_{e,max}$). All four data kinds do include information concerning pressure, mass velocity, and tube diameter, providing sufficient information to develop CHF correlations. For the first data kind, all parameters provided are experimentally measured and therefore readily available for assessment of any anomalies. For the second kind of data, critical thermodynamic quality is found using Eq. (17) and checked to make certain $x_{e,CHF} \leq 1$. Data which do not obey this requirement are presented in Table 3. For the third kind of data, the inlet thermodynamic quality and inlet temperature are found using Eq. (17) and finding $T_{in} = f(P, h_{in})$. For certain LHe data points from Ogata and Sato [57], inlet temperature was found to be smaller than the Lambda Temperature (2.17 K), the transition temperature between He I and He II, the latter being a zero viscosity "superfluid" whose complex physical behavior is beyond the scope of the present study. Since Ogata and Sato [57] were concerned with He I data alone, the He II data were excluded, as indicated in Table 3. Before addressing the fourth kind of data, it is important to note that, for a fixed mass velocity, diameter and pressure, $x_{e,CHF}$ is unique for a given CHF value, with inlet quality, $x_{e,in}$, and critical length, L_{CHF}, acting as dependent variables governed by Eq. (17). Hence, the unknown information of L_{CHF} and $x_{e,in}$ is determined by (a) either *fixing* L_{CHF} to be the same as the entire heated length, L_H, and determining $x_{e,in}$ using Eq. (17) and checking if $x_{e,in} \geq x_{e,min}$, or (b) *fixing the* $x_{e,in}$ to be the same as $x_{e,min}$ if $x_{e,in}$ from the previous method is less than $x_{e,min}$ specified in the operational range, then determining L_{CHF} using Eq. (17) and checking if $L_{CHF} \leq L_H$. It can be seen that irrespective of the different permutations of $x_{e,in}$ and L_{CHF}, until they obey Eq. (17) and give the same $x_{e,CHF}$ as reported in the literature for a given combination of mass velocity, diameter and pressure, and satisfy the inequalities, $x_{e,min} \leq x_{e,CHF} \leq x_{e,max}$ and $L_{CHF} \leq L_H$, they will have a CHF value identical to that reported in the literature. No data were found that showed any anomalies or failed to satisfy either method (a) or method (b) while adhering to all the inequalities, in addition to satisfying constant pressure assumption.

CHF for flow in a uniformly heated tube is generally believed to occur near the outlet. However, a significant number of data points were found where CHF occurred at a location between the inlet and outlet. However, a few deviations have been observed in some of the data by Yarmak and Zhukov [70], Romanov *et al.* [69], and Petukhov *et al.* [60], which had both $x_{e,in}$ and $x_{e,CHF}$ reported, in which case L_{CHF} was found using Eq. (17). In the present CHF Database, it is mandated that $L_{CHF} \leq L_H$ and, for CHF occurring at the outlet, $L_{CHF} = L_H$. Table 3 indicates data that are excluded because the indicated L_{CHF} was listed in original references as exceeding L_H.

3.3. Final PU-BTPFL Cryogen Flow Boiling CHF Database

The final PU-BTPFL Cryogen Flow Boiling CHF Database, which includes all data deemed acceptable for development of CHF correlations, is arrived at after applying all the exclusion criteria outlined in the previous section. Details of the database are provided in Table 4. Overall, the CHF database has 2312 useable CHF data points conforming to the functional forms of Eqs. (5) and (6) and therefore acceptable for correlation development. Overall, the database encompasses four different fluids: liquid hydrogen, LH_2, liquid helium, LHe, liquid nitrogen, LN_2, and liquid methane, LCH_4. In Table 4, the upper and lower numbers for each parameter represent minimum and maximum values, respectively, for accept-

Table 3
Summary of data points deemed unreliable and therefore excluded from the CHF Database due to energy balance related violations.

Reference	Total CHF data points	$x_{e,CHF} > 1$[a]	$L_{CHF} > L_H$[b]	$T_{in} < T_\lambda$[c]	Acceptable CHF data points
Liquid Hydrogen					
(a) Vertical Upflow					
Lewis *et al.* [55]	92	16			76
Liquid Helium					
(a) Vertical Upflow					
Ogata and Sato [57]	27			3	24
Beliakov *et al.* [68]	89	1			88
Romanov *et al.* [69]	28		1		27
Petukhov *et al.* [60]	2		1		1
Yarmak and Zhukov [70]	11		2		9
Liquid Nitrogen					
(a) Vertical Upflow					
Grigoriev *et al.* [54]	7	2			5
Petukhov *et al.* [60]	2		1		1
		19	**5**	**3**	

[a] Applicable to data points where exit quality is determined from prescribed inlet conditions
[b] Applicable to data points where CHF location is determined from prescribed inlet and critical (local) qualities
[c] Applicable to only LHe data points where inlet quality is evaluated from prescribed CHF location and critical quality

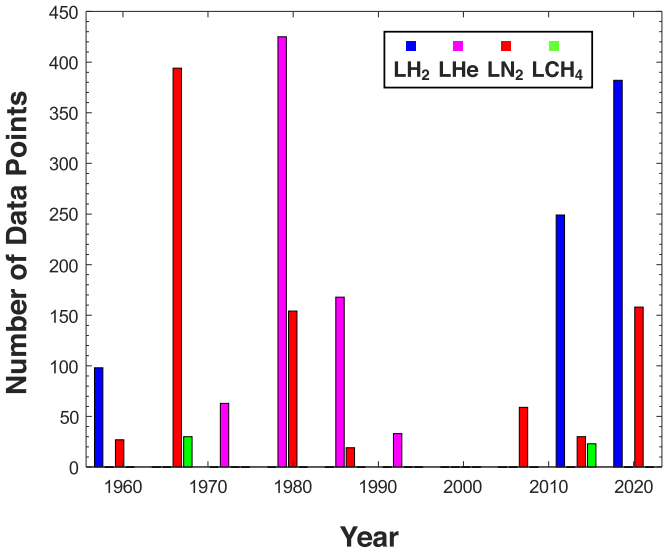

Fig. 6. Timeline for cryogen flow boiling CHF data measurements over past 60 years.

able CHF data corresponding to a particular reference. It is important to re-emphasize that the entire database is (a) for uniformly heated round tubes (excludes any quenching data), and (b) includes only horizontal, vertical upflow, and vertical downflow, and therefore excludes all other intermediate flow orientations. With a total of 2,312 data points, it is the largest database ever consolidated from the literature for cryogens.

4. Parametric Distribution of PU-BTPFL Cryogen CHF Database

As indicated in the previous section, the PU-BTPFL Cryogen CHF Database, referred to hereafter as CHF Database, contains over 2,312 CHF data points, segregated according to different cryogens.

Figure 6 shows a 60-year timeline during which cryogen flow boiling CHF data (from the present CHF Database) were measured. Despite seemingly fairly well distributed efforts over this period, notice how more emphasis has been placed on specific cryogens during relatively shorter time spans. This trend can be explained by applications of interest during a particular duration. For example, after initial period of academic research interest in LHe I heat transfer in West Germany [56], United States of America [89], and Japan [57,58] in the early 1970s, the decade of 1975-85 was a golden age for LHe flow boiling research in the Soviet Union in connection with the development of forced convective cooling of superconducting systems [59,68,69,83,84,85,87,60]. The decade post 2008 saw a surge in LH_2 flow boiling research primarily done in Japan with the objective of cooling large scale high temperature superconductor (HTS) magnets [65,72,73,74,75,76,77,78,79,80]. Apart from the conscious work carried out in Japan to compare the results of LH_2 and LN_2 [65,92,94], research on LN_2 has been more academic in nature, performed with varied importance throughout the years. And, following some work around 1960, LCH_4, received renewed interest in the late 2010 at the NASA Glenn Research Center [97] as part of their Propulsion and Cryogenics Advanced Development (PCAD) project, where nontoxic propellants such as LOX/LCH_4 were being tested for spacecraft applications. Another obvious feature of the data in Fig. 6 is the greater overall emphasis investigators have placed on LN_2, followed, in order, by LH_2 and LHe, with LCH_4 receiving the least emphasis. It must be mentioned that flow boiling research of cryogenics has not been limited to these four fluids as there are heat transfer coefficient and pressure drop data available sporadically in the literature for Liquid Neon, LNe, Liquid Carbon Monoxide, LCO, Liquid Argon, LAr, and Liquid Oxygen, LOX. Unfortunately, the authors were not able to find CHF data for these fluids in the open literature, though some data might be available in proprietary databases of national laboratories or research organizations across the globe.

Discussed next are operating conditions where few CHF data points exist. Figures 7(a)-(j) show distribution of data (within the CHF Database) based on the basic operational parameters of (a) system pressure, (b) reduced pressure, (c) inlet subcooling, (d) inlet quality, (e) mass velocity, (f) tube inner diameter, (g) heated length-to-diameter ratio, (h) tube wall thickness, (i) tube wall thermal conductivity, and (i) flow orientation angle. For each of these parameters, the data distribution is segregated based on fluid. Figure 7(a) shows, for all cryogens, far more data are available for lower pressures. However, this might be misleading given the large variations in critical pressure for the different cryogens. The pressure distribution is better presented by plotting the data against reduced pressure, Fig. 7(b), which shows more overall data uniformity in terms of the reduced pressure distribution. But, Fig. 7(b) also shows more emphasis for LN_2 on lower reduced pressures, compared to a more uniform distributions for LH_2 and LCH_4, and

Table 4
Parameter ranges of acceptable CHF data with prescribed inlet conditions and/or critical (local[a]) conditions

Reference	Acceptable CHF data	Tube dimensions			Operating Conditions		Inlet Conditions		Critical (local[a]) Conditions				CHF	Remarks
		D x 10^3 [m]	L_H/D [-]	L_{CHF}/D [-]	P x 10^{-6} [N m^{-2}]	G [kg m^{-2} s^{-1}]	$\Delta T_{sub,in}$ [K]	$x_{e,in}$ [-]	$\Delta P_{max}/P$ [-]	$\Delta T_{sub,CHF}$ [K]	$x_{e,CHF}$ [-]	α_{CHF} [b] [-]	q_{CHF} x 10^{-3} [W m^{-2}]	
Liquid Hydrogen														
(a) *Vertical Upflow*														
von Glahn and Lewis [71]	21	14	29.3	2.8	0.34	5.6	1.4	-0.04	0	0	0.12	0.45	19.1	SS 347 Tube
		14	29.3	29.3	0.34	13.3	1.4	-0.04	0	0	0.96	0.99	78.5	$t_w = 0.9$ mm
Lewis *et al.* [55]	76	14.1	29.1	2.5	0.21	3.9	0	-0.18	0	0	0.04	0.2	18.6	SS 304 Tube
		14.1	29.1	29.1	0.54	23	5.5	0	0	0	1	1	76.8	$t_w = 0.9$ mm
Tatsumoto *et al.* [72]	23	3	33.3	33.3	0.7	156.5	0	-0.33	0	0	-0.26	0	34.9	SS 304 Tube
		3	33.3	33.3	0.7	1663.4	8	0	0.08	5.9	0.1	0.27	391.1	$t_w = 0.5$ mm
Shirai *et al.* [73]	3	6	16.8	16.8	0.4	63.6	5.2	-0.16	0	1.1	-0.07	0	39.4	SS Tube
		6	16.8	16.8	0.4	282.6	5.2	-0.16	0	2.1	-0.04	0	141	$t_w = 0.2$ mm
Tatsumoto *et al.* [74]	3	6	16.7	16.7	0.7	106	8	-0.33	0	2.4	-0.26	0	105.3	SS 304 Tube
		6	16.7	16.7	0.7	897.8	8	-0.33	0	5.7	-0.13	0	324.4	$t_w = 0.2$ mm
Shirai *et al.* [75]	21	6	16.8	16.8	0.7	65.3	0	-0.33	0	0	-0.26	0	54.5	SS 304 Tube
		6	16.8	16.8	0.7	897.2	8	0	0	5.7	0.16	0.39	339	$t_w = 0.2$ mm
Shirai *et al.* [76]	41	6	16.7	16.7	0.4	61.2	0	-0.55	0	0	-0.47	0	28.7	SS 304 Tube
		6	16.7	16.7	1.1	897.5	8	0	0	5.8	0.16	0.4	339.7	$t_w = 0.2$ mm
Tatsumoto *et al.* [77]	14	6	33.3	33.3	0.7	68.1	0	-0.33	0	0	-0.23	0	23.3	SS 316 Tube
		6	33.3	33.3	0.7	832.3	8	0	0.01	5	0.14	0.36	218.7	$t_w = 0.2$ mm
Tatsumoto *et al.* [78]	112	4	8.3	8.3	0.4	26	0	0	0	0	0.02	0.05	7.5	SS 316 Tube
		6	41.8	41.8	1.1	903.1	0	0	0.04	0	0.18	0.44	155.8	$t_w = 0.5$ mm
Shirai *et al.* [65]	380	3	8.3	8.3	0.4	17.3	0	-0.89	0	0	-0.8	0	9.6	SS 316L Tube
		9	50	50	1.1	2620.2	11	0	0.16	9	0.28	0.51	429.6	$t_w = 0.2$ – 0.5 mm
Matsumoto *et al.* [79]	2	8	25	25	0.7	140	0	0	0	0	0.05	0.17	45.6	SS 310S Tube
		8	25	25	0.7	340	0	0	0	0	0.1	0.28	60.6	
	696													
(b) *Horizontal flow*														
Wright and Walters[c] [66]	1	6.4	24	24	0.16	418	0	0.01	0.08	0	0.04	0.31	60.4	Copper Tube
		6.4	24	24	0.16	418	0	0.01	0.08	0	0.04	0.31	60.4	$t_w = 6.4$ mm
Tatsumoto *et al.* [80]	32	3	16.7	16.7	0.7	138.5	0	-0.33	0	0	-0.28	0	74	SS 304 Tube
		6	33.3	33.3	0.7	2642.9	8	0	0.11	6.3	0.11	0.3	483.4	$t_w = 0.2$ mm
	33													
LH_2 CHF data points	**729**													
Liquid Helium														
(a) *Vertical Upflow*														
Johannes [81]	10	2.1	139.6	139.6	0.11	58.9	0.1	-0.17	0	0	0.2	0.39	1.3	Monel Tube
		2.1	139.6	139.6	0.15	245.7	0.5	-0.03	0.02	0	0.58	0.83	2.8	$t_w = 0.1$ mm
Hilderbrandt [56]	3	1	20	20	0.08	5.6	0	0	0	0	0.09	0.3	1	Silver Block
		1	20	20	0.08	76.3	0	0	0	0	0.66	0.9	1.8	$\varepsilon = 0.1$ μm
Ogata and Sato [57]	24	1.1	78	78	0.11	79.3	0	-1.11	0	0	-0.16	0	0.1	SS Tube
		1.1	78	78	0.2	321.5	2.8	0.84	0.01	0.1	1	1	5.5	$t_w = 0.3$ mm
Ogata and Sato [58]	8	1.1	78	51.4	0.11	78.8	0	-0.39	0	0	0	0	0.5	SS Tube
		1.1	78	51.4	0.19	92.2	0.7	0.5	0	0	0.57	0.78	3.9	$t_w = 0.3$ mm
Keilin [82]	3	2	50	50	0.12	39.8	0	0	0	0	0.88	0.96	0.9	Copper Tube
		2	50	50	0.12	39.8	0	0.65	0	0	0.97	0.99	3.6	

(*continued on next page*)

Table 4 (*continued*)

Reference	Acceptable CHF data	Tube dimensions			Operating Conditions		Inlet Conditions		Critical (local[a]) Conditions				CHF	Remarks
		D x 10^3 [m]	L_H/D [-]	L_{CHF}/D [-]	P x 10^{-6} [N m^{-2}]	G [kg m^{-2} s^{-1}]	$\Delta T_{sub,in}$ [K]	$x_{e,in}$ [-]	$\Delta P_{max}/P$ [-]	$\Delta T_{sub,CHF}$ [K]	$x_{e,CHF}$ [-]	α_{CHF} [b] [-]	q_{CHF} x 10^{-3} [W m^{-2}]	
Grigoriev *et al.* [54]	15	0.7	194	194	0.01	13.8	0	0	0	0	0.59	0.85	0.4	SS Tube
		0.7	194	194	0.1	181.5	0	0	0.13	0	1	1	2.5	$t_w = 0.2$ mm
Arkhipov *et al.*[d] [83]	36	1.6	110.4	19.9	0.1	83	0.2	-0.25	0	0	-0.07	0	1.2	SS Tube
		1.6	110.4	110.4	0.2	314	1.6	-0.08	0.02	0.1	0.39	0.7	5.1	
Beliakov *et al.* [68]	88	4.1	-	5	0.12	2.2	0	0	0	0	0.02	0.05	0.7	SS Tube
		4.1	-	34	0.18	199.9	0	0.84	0.01	0	0.92	0.97	5	$t_w = 0.2$ mm
Deev *et al.* [84]	108	1.6	110.4	30	0.11	92	0	-0.32	0	0	-0.05	0	0.2	SS Tube
		1.6	110.4	107	0.12	305	2.1	0.89	0.04	0.2	0.9	0.97	7.2	
Petukhov *et al.* [59]	4	0.8	226.3	67.2	0.1	60	0	-0.01	0	0	0.25	0.56	0.1	SS Tube
		0.8	226.3	192.9	0.1	300	0.1	0.45	0.08	0	0.48	0.78	2.5	$t_w = 0.1$ mm
Petukhov *et al.*[d] [59]	55	0.8	226.3	8.1	0.1	60	0	0	0	0	0.05	0.17	0.1	SS Tube
		0.8	226.3	226.3	0.1	313	0	0.6	0.12	0	0.7	0.9	6.7	$t_w = 0.1$ mm
Romanov *et al.* [69]	27	0.5	212.8	15.4	0.1	22	0	0	0	0	0.07	0.23	0.5	-
		0.5	212.8	209.5	0.1	275	0	0	0.09	0	0.88	0.96	4.4	
Subbotin *et al.*[d] [85]	92	1.6	110.4	37.2	0.1	85	0	-0.25	0	0	0.02	0.05	0.05	SS Tube
		1.6	110.4	110.4	0.18	315	1.4	0.67	0.03	0	0.69	0.87	5.1	
Katto [86]	138	1	25	25	0.2	10.5	0	-0.62	0	0	-0.19	0	0.1	SS Tube
		1	200	200	0.2	107.6	1.1	0.32	0	0.2	0.93	0.96	3.5	$t_w = 0.3$ mm
Subbotin *et al.*[d] [87]	29	1.6	110.4	34.8	0.12	86	0	-0.25	0	0	-0.05	0	0.05	SS Tube
		1.6	110.4	110.4	0.18	211	1.3	0.95	0.01	0.1	0.96	0.99	4.3	
Petukhov *et al.* [60]	1	1.8	72.2	67.2	0.1	90	0	0	0	0	0.36	0.68	2.5	SS Tube
		1.8	72.2	67.2	0.1	90	0	0	0	0	0.36	0.68	2.5	$t_w = 0.1$ mm
Yarmak and Zhukov [70]	12	0.8	187.5	3	0.1	78	0	0	0	0	0.02	0.07	1.5	SS Tube
		0.8	187.5	121.8	0.1	235	0	0	0.02	0	0.45	0.75	4.5	$t_w = 0.1$ mm
	653													
(b) *Horizontal flow*														
Bredy[e] [88]	1	10	10	10	0.1	76.4	0	0	0	0	0.27	0.59	10.7	SS Tube
		10	10	10	0.1	76.4	0	0	0	0	0.27	0.59	10.7	
	1													
(c) *Vertical Downflow*														
Giarrantano *et al.* [89]	15	2.1	46.9	16.7	0.11	48	0	-0.38	0	0	-0.05	0	1.6	SS Tube
		2.1	46.9	45.4	0.21	636	0.2	0.02	0.03	0	0.38	0.69	5.3	$t_w = 0.2$ mm
Giarrantano *et al.* [90]	20	2.1	46.9	2.5	0.11	45	0	-0.3	0	0	-0.22	0	1.6	SS Tube
		2.1	46.9	45.1	0.2	630	0.3	0	0.03	0.2	0.4	0.7	6.9	$t_w = 0.2$ mm
	35													
LHe CHF data points	**689**													
Liquid Nitrogen														
(a) *Vertical Upflow*														
Lewis *et al.* [55]	27	14.1	29.1	3	0.33	21	0.7	-0.04	0	0	0.08	0.54	28	SS 304 Tube
		14.1	29.1	29.1	0.39	73	3.2	-0.01	0	0	0.93	0.99	81.4	$t_w = 0.9$ mm
Papell *et al.* [91]	170	12.8	23.8	23.8	0.34	103	6.7	-0.51	0	0	-0.39	0	79.1	Nickel Alloy Tube
		12.8	23.8	23.8	1.65	2553	28.3	-0.08	0.02	20.7	0.89	0.99	430	$t_w = 0.3$ mm

(*continued on next page*)

Table 4 (*continued*)

Reference	Acceptable CHF data	Tube dimensions			Operating Conditions		Inlet Conditions		Critical (local[a]) Conditions				CHF	Remarks
		D x 10^3 [m]	L_H/D [-]	L_{CHF}/D [-]	P x 10^{-6} [N m^{-2}]	G [kg m^{-2} s^{-1}]	$\Delta T_{sub,in}$ [K]	$x_{e,in}$ [-]	$\Delta P_{max}/P$ [-]	$\Delta T_{sub,CHF}$ [K]	$x_{e,CHF}$ [-]	α_{CHF} [b] [-]	q_{CHF} x 10^{-3} [W m^{-2}]	
Grigoriev *et al.* [54]	5	0.7	104	104	0.1	38.9	0	0	0.01	0	0.92	1	19.4	-
		1.3	194	194	0.1	135.9	0	0	0.12	0	1	1	59.7	
Katto and Yokoya [86]	18	1	200	200	0.22	109	0.8	-0.05	0.02	0	0.79	0.99	21.1	SS 304 Tube
		1	200	200	0.22	328	4.5	-0.01	0.17	0	0.99	1	79.4	$t_w = 0.3$ mm
Petukhov *et al.* [60]	1	1.8	72.2	69.9	0.1	170	0	0	0.06	0	0.33	0.94	40.3	SS Tube
		1.8	72.2	69.9	0.1	170	0	0	0.06	0	0.33	0.94	40.3	$t_w = 0.1$ mm
Zhang and Fu [62]	1	1	96	96	0.12	185.8	1.7	-0.02	0.06	0	0.13	0.81	14	SS 304 Tube
		1	96	96	0.12	185.8	1.7	-0.02	0.06	0	0.13	0.81	14	
Tatsumoto *et al.* [92]	30	5.4	18.5	18.5	0.5	80.9	4.9	-0.76	0	0	-0.65	0	44.5	SS 304 Tube
		5.4	18.5	18.5	2	3504	37.5	-0.06	0.01	31.1	0.3	0.82	330.9	$t_w = 0.3$ mm
Shirai *et al.* [65]	121	3	16.7	16.7	0.5	309.5	0	-0.37	0	0	-0.31	0	29.6	SS 316L Tube
		6	41.8	41.8	1	8203.9	25.7	0	0.17	21.2	0.11	0.49	1012.4	$t_w = 0.2$ – 0.5 mm
Zhang *et al.* [63]	1	1.3	230.8	230.8	0.9	2010	25.2	-0.35	0.02	10.7	-0.15	0	65.6	SS 304 Tube
		1.3	230.8	230.8	0.9	2010	25.2	-0.35	0.02	10.7	-0.15	0	65.6	$t_w = 0.9$ mm
Zhang *et al.* [64]	3	2	148.2	129.8	0.63	680	16.2	-0.29	0.01	0	0.48	0.85	149.2	SS 321 Tube
		2	148.2	129.8	1.08	680	19.2	-0.21	0.04	0	0.65	0.94	187.4	$t_w = 1$ mm, $\varepsilon = 7.2$ μm
	377													
(b) *Horizontal flow*														
Steiner and Schlünder [d] [67]	5	14	37.5	34.7	0.91	44	0	0.02	0	0	0.5	0.87	23.7	Copper Tube
		14	37.5	37.5	0.91	452	0	0.43	0	0	0.7	0.94	35.3	$t_w = 3$ mm, $\varepsilon = 0.1$ μm
Müller *et al.* [d] [93]	144	14	37.5	9.3	0.11	44	0	0	0	0	0.07	0.2	11.5	Copper Tube
		14	37.5	37.5	3.06	470	0	0.86	0.14	0	0.99	1	111.1	$t_w = 3$ mm, $\varepsilon = 0.1$ μm
Yun *et al.* [61]	3	10.6	155.7	26	0.17	56.2	0	0	0	0	0.32	0.91	33.6	SS Tube
		10.6	155.7	103.7	0.17	85.6	0	0	0.01	0	0.84	0.99	33.6	
Tatsumoto *et al.* [94]	55	5.4	18.5	18.5	0.5	59.1	4.9	-0.36	0	0	-0.29	0	29.8	SS 304 Tube
		5.4	18.5	18.5	1	2700.8	25.6	-0.06	0	19.8	0.47	0.85	250.2	$t_w = 0.3$ mm
Liu *et al.* [95]	33	2.9	205	205	0.2	134.4	0	0	0.01	0	0.63	0.96	19.3	SS Tube
		2.9	205	205	0.35	343.7	0	0.01	0.13	0	0.73	0.98	56.1	
	240													
(c) *Vertical Downflow*														
Papell *et al.* [91]	224	12.8	23.8	23.8	0.34	110.3	6.7	-0.51	-0.01	0	-0.41	0	15	Nickel Alloy Tube
		12.8	23.8	23.8	1.65	2589.2	28.3	-0.08	0	22.3	0.25	0.82	427.7	$t_w = 0.3$ mm
	224													
LN_2 CHF data points	**841**													
Liquid Methane														
(a) *Vertical Upflow*														
Glickstein and Whitesides [d] [96]	30	8.5	98.5	18.1	1.03	225.8	42.6	-1.06	0	1.2	-0.73	0	342	Inconel 600 Tube
		8.5	98.5	98.5	2.99	3702.6	71.6	-0.38	0.02	46	-0.01	0	1755.8	$t_w = 0.4$ mm
Van Noord [97]	23	1.4	60.2	60.2	1.75	2858.8	42.4	-2.06	0.01	0	-1.23	0	2010.1	Inconel 600 Tube
		2.1	89.3	89.3	4.07	7017	78.9	-0.45	0.04	48.5	0.21	0.54	8203.9	$t_w = 0.5$ – 0.6 mm
LCH_4 CHF data points	**53**													
Grand Total	**2312**													

[a] Local condition are specified at axial location of CHF. For CHF occurring at the exit, exit conditions are the same as local conditions.
[b] Evaluated using Zivi's void fraction equation, Eq. (12). Test cases with critical void fraction equal to zero signify occurrence of DNB type CHF.
[c] Data extracted from Steiner and Schlünder [67]
[d] Data with known critical quality, heated length, and minimum value of local thermodynamic equilibrium quality in experiments. See section 3.2 for details.
[e] Tube at an orientation of 4° from the horizontal plane and considered (quasi-) horizontal in this study

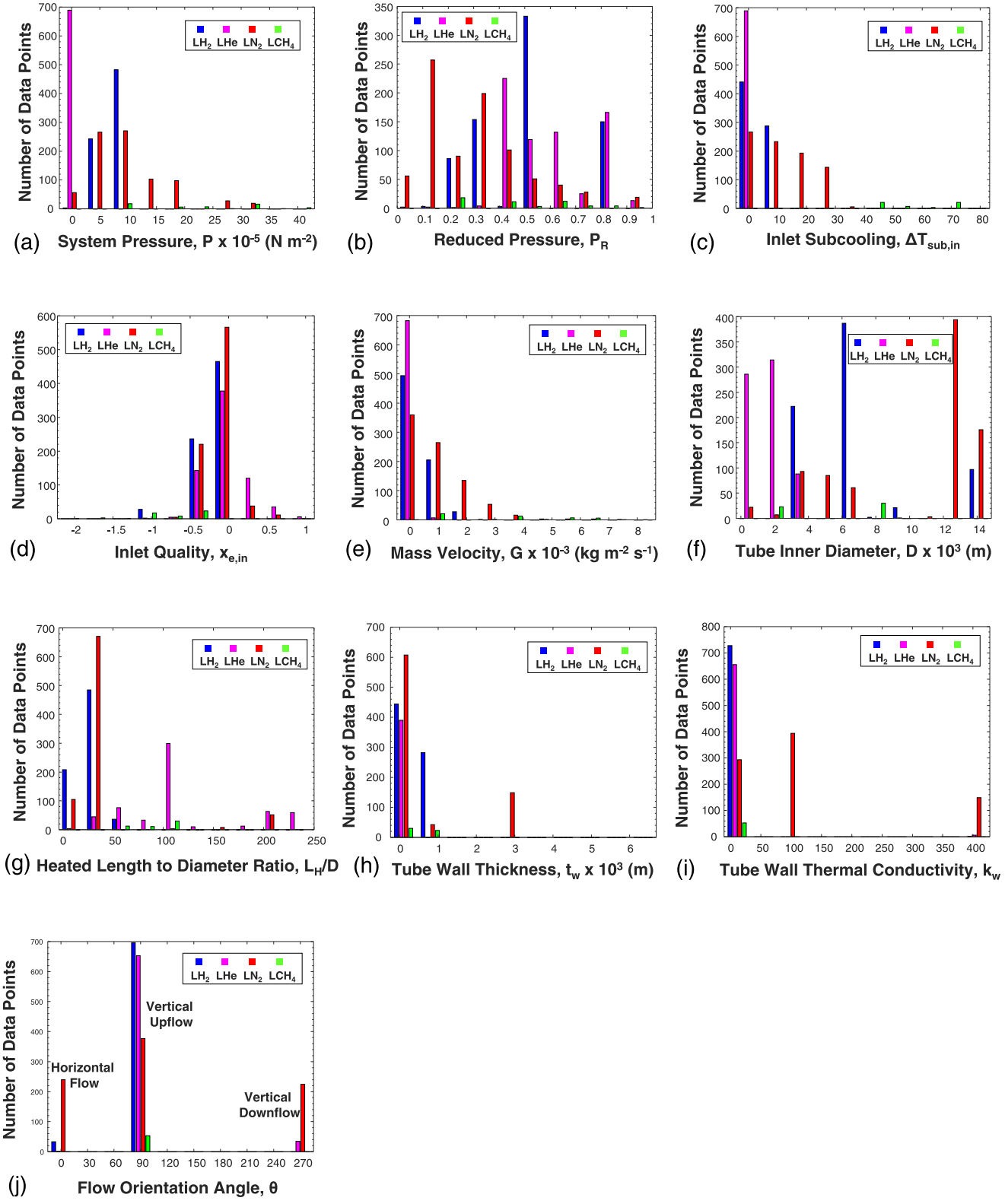

Fig. 7. Distribution of data in the CHF Database relative to (a) system pressure, (b) reduced pressure, (c) inlet subcooling, (d) inlet quality, (e) mass velocity, (f) tube diameter, (g) heated length to diameter ratio, (h) tube wall thickness, (i) tube wall thermal conductivity, and (j) flow orientation angle.

higher reduced pressure emphasis for LHe. Figure 7(c) shows relatively narrow distribution for inlet subcooling (below 10 K) for both LH_2 and LHe, compared to a broader range of up to ~ 30 K for LN_2 and much higher subcoolings (some exceeding 70 K) for LCH_4. Better representation of inlet thermodynamic state is provided in Fig 7(d) which shows the data encompassing both subcooled and saturated inlet conditions. Figure 7(e) shows more data available for mass velocity values up to ~ 3,000 kg/m^{2}s and far less above this value. Figure 7(f) shows a broad distribution versus tube diameter, with LHe data clustered towards small diameters of

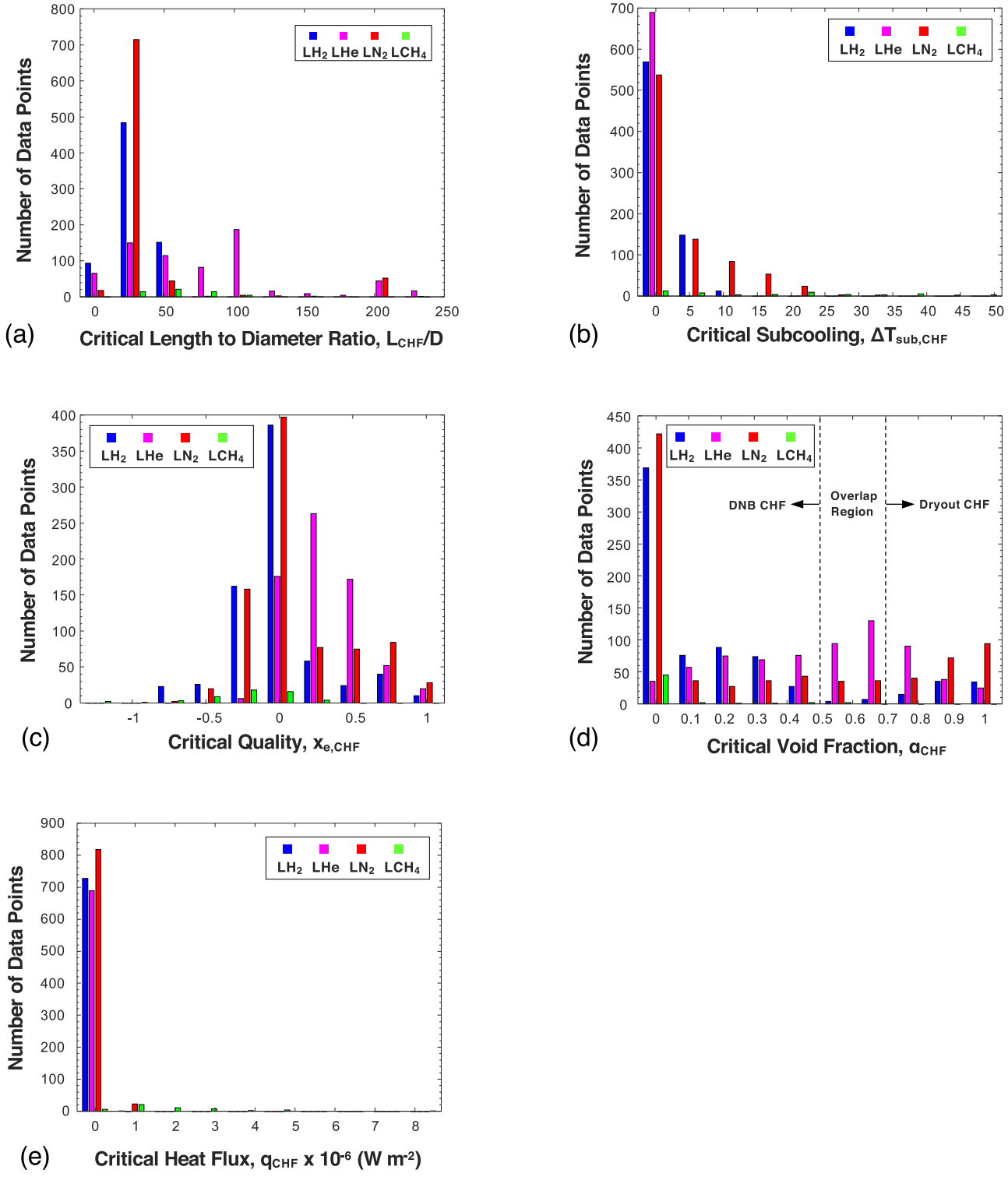

Fig. 8. Distribution of data in the CHF Database relative to (a) critical length to diameter ratio, (b) critical subcooling, (c) critical quality, (d) critical void fraction, and (e) measured CHF.

less than ~ 4 mm, versus broader distributions for the other three cryogens. Figure 7(g) shows the vast majority of data is available for heated length to diameter ratios below ~ 100. Figures 7(h) and 7(i) are included here for completeness though tube wall thickness and thermal conductivity information provided little guidance in terms of correlating CHF data. Figure 7(h) shows most studies employed tube wall thicknesses below 1 mm, except for some LN_2 data, which used tubes with ~ 3-mm thickness. Figure 7(h) shows almost all the data were obtained using tubes made from a variety of stainless steel alloys (~ 16.2 W/m-K), while some data employed nickel alloys (~ 100 W/m-K) and fewer used copper or silver (~ 400 W/m-K). Finally, Fig. 7(j) shows the majority of CHF data were obtained in vertical upflow, with LN_2 data present in all three flow orientations and LCH_4 data only vertically upflow.

Figures 8(a)-(e), show distribution of the data based on the parameters closely associated with CHF: (a) critical length to diame-

ter ratio, (b) critical subcooling, (c) critical quality, (d) critical void fraction, and (e) measured CHF. Figures 8(a) shows the vast majority of data is available for critical length (axial location where CHF is experimentally identified) to diameter ratios below ~ 100. Figure 8(b) shows that all the data for LH_2 and LHe have either zero or very low critical subcooling (defined using fluid temperature at the axial location where CHF is experimentally identified), and LN_2 and LCH_4 associated with high subcooling at CHF location. Figure 8(c) shows critical quality distribution encompassing both subcooled and saturated conditions. Figure 8(d) shows a quantitative representation of void fraction at the CHF location, evaluated using Eq. (12). Except for LCH_4 data, which has mostly near-zero void fraction all along, all other fluids show uniform scatter for all positive void fraction range. Since there are data points with negative critical qualities, signifying DNB-type CHF, the void fractions for these data pointed are noted as having zero value. Finally, Fig. 8(e) shows increasing CHF values for LHe, LH_2, and LN_2, in order, over a range well below ~ 100 W/m^2, compared to much broader range for LCH_4.

Figures 9(a)-(c) show distribution of data based on (a) maximum pressure drop ratio, (b) confinement number, and (c) modified Froude number. Figure 9(a) shows all data in the CHF Database satisfy the constant pressure drop criteria of $0.1 \leq \Delta P_{max}/P \leq 0.2$. Figure 9(b) shows that almost all of the CHF data are associated with Confinement numbers below 0.5, while a few LN_2 and LCH_4 data points do exceed this value. Notice that, with *Co* inversely dependent on tube diameter, high *Co* values are also reflected in high pressure drop across the tube. Figure 9(c) highlights the ability of LH_2 to exhibit high values of modified Froude number, Fr^*, compared to other fluids, an inference which was also made in conjunction with Fig. 4(c). The main implication of high Fr^* for LH_2 is strong dominance of inertial effects over gravity/buoyancy effects, rendering the flow physics, including CHF, independent of flow orientation.

Aside from insight into details of the CHF database, Table 4 and Figs. 7-9 serve to guide future experimental research into filling significant gaps in cryogen data in an effort to both maximize new data yield and minimize unnecessary future experimental expenditures. Following is a summary of major experimental needs based on the gaps identified in the CHF Database:

1 Critical need for more CHF data for Liquid Oxygen, LOX, along with additional data for LCH_4.
2 Additional data for Horizontal flow and vertical downflow.
3 Additional data for Dryout-type CHF.
4 Additional data for large heated length-to-diameter ratios.
5 More high mass velocity data.
6 Systematic tests to investigate the parametric effects of wall thickness, wall thermal conductivity, surface roughness and surface ageing on CHF.

5. Development of Universal CHF Correlations

With the CHF data now vetted against all possible physics violations and tested for constant pressure approximation, a detailed plan is adopted to develop universal CHF correlations. As mentioned in section 1.4, three classifiers: (1) fluid, (2) CHF type (Dryout versus DNB), and (3) flow orientation, will affect the magnitude of CHF. As seen from Table 4, CHF values for LHe are orders of magnitude lower than for LH_2 and LN_2 which, in turn, are lower than for LCH_4. Similarly, for low mass velocities, orientation effects play a major role in either preponing or postponing CHF. But the most important classifier is the CHF mechanism since the flow regimes and associated fluid physics leading to CHF are completely different for different fluids and different flow orientations. Hence, it is imperative to classify the data

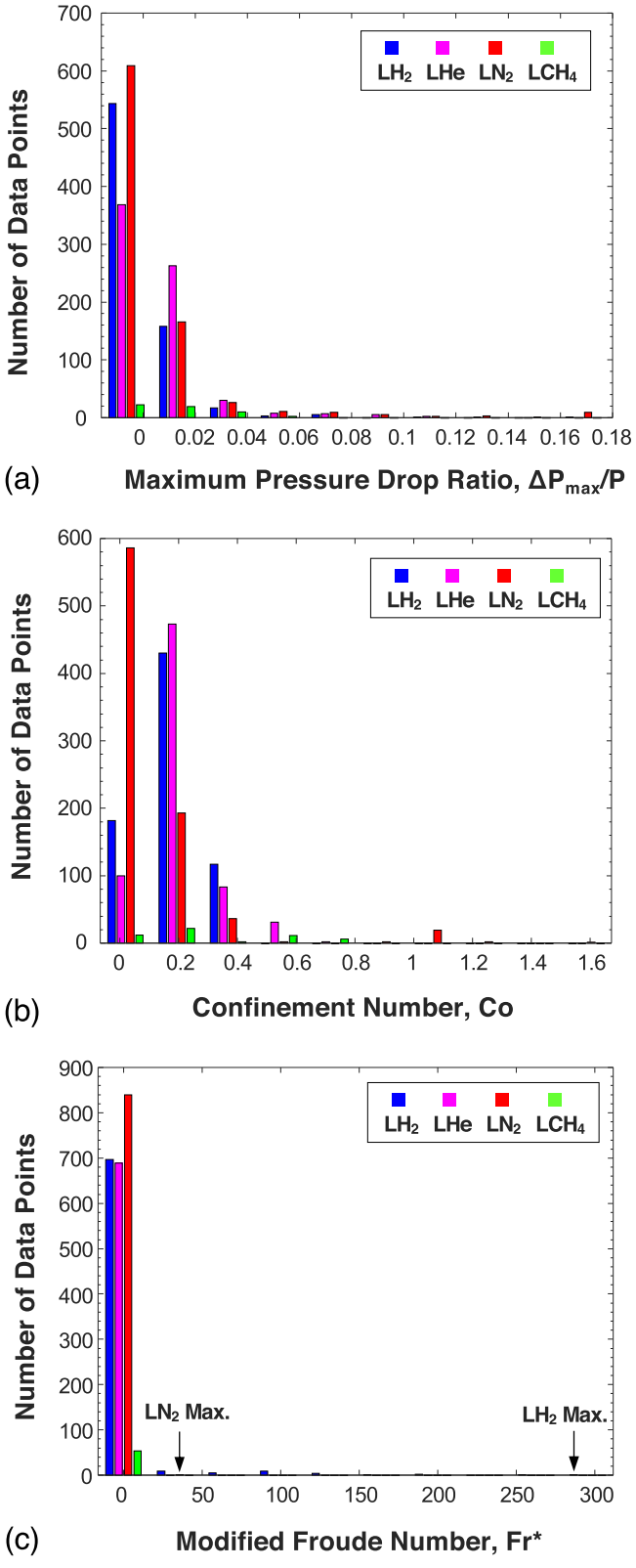

Fig. 9. Distribution of data in the CHF Database relative to (a) maximum pressure drop ratio, (b) confinement number, and (c) modified Froude number.

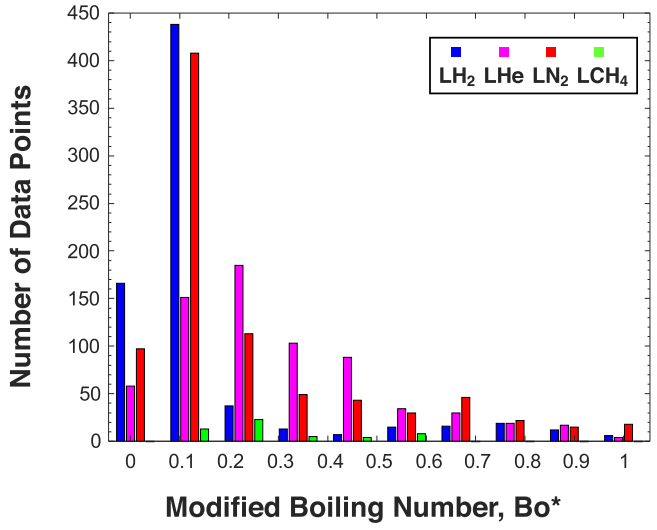

Fig. 10. Distribution of data in the CHF Database relative to modified boiling number, Bo^*.

based on CHF mechanism before proceeding with the correlation development.

5.1. Segregation of Database into DNB versus Dryout

As seen from Fig. 5, DNB is characterized by high mass velocity, high magnitude of CHF, high inlet subcooling or low inlet quality, and low critical length to diameter ratio; these conditions lead to high CHF magnitude for DNB. On the other hand, Dryout is characterized by parameter trends opposite to those for DNB, *i.e.,* low mass velocity, low magnitude of CHF, low inlet subcooling or high inlet quality, and high critical length to diameter ratio, which lead to comparatively low CHF magnitude for Dryout.

One drawback in using Boiling number ($Bo = q_{CHF}/(Gh_{fg})$) to distinguish the two CHF types is that it tends to cancel out the effects of high CHF and high mass velocity for DNB, as well as low CHF and low mass velocity for Dryout. With the limited value of Bo in aiding to determination of the CHF mechanism, a modified Boiling number, Bo^*, is proposed which is arrived at by re-arranging Eq. (17),

$$Bo^* = \frac{4Bo\frac{L_{CHF}}{D}}{1 - x_{e,in}} = \frac{x_{e,CHF} - x_{e,in}}{1 - x_{e,in}}, \tag{18}$$

which varies from 0 – 1. The denominator in Bo^* allows this dimensionless parameter to acquire higher values for Dryout versus lower values for DNB. It is therefore an effective tool for distinguishing the CHF types. Figure 10 shows the distribution of data in the CHF Database relative to the modified Boiling number.

Rearranging Eq. (18) results in a linear function of critical quality,

$$Bo^* = \frac{1}{1 - x_{e,in}} x_{e,CHF} + \frac{-x_{e,in}}{1 - x_{e,in}}. \tag{19}$$

Both the slope and the intercept of this linear function are dependent on inlet quality alone. In the limiting case of saturated liquid inlet, $x_{e,in} = 0$, Eq. (19) reduces to $Bo^* = x_{e,CHF}$.

The effectiveness of Eq. (19) is put to test by plotting measured Bo^* versus measured critical quality in Figs. 11(a)-(d) for LH_2, LHe, LN_2, and LCH_4, respectively. Clear demarcation lines are captured in these figures: (i) $Bo^* = x_{e,CHF,}$ which is the locus for data with $x_{e,in} = 0$, (ii) $x_{e,CHF} = 0$, which identifies all data points definitely undergoing DNB by satisfying the criteria $x_{e,CHF} \leq 0$, and (iii) $Bo^*_{DNB,max}$, which is the maximum value for DNB data ($x_{e,CHF} \leq 0$),

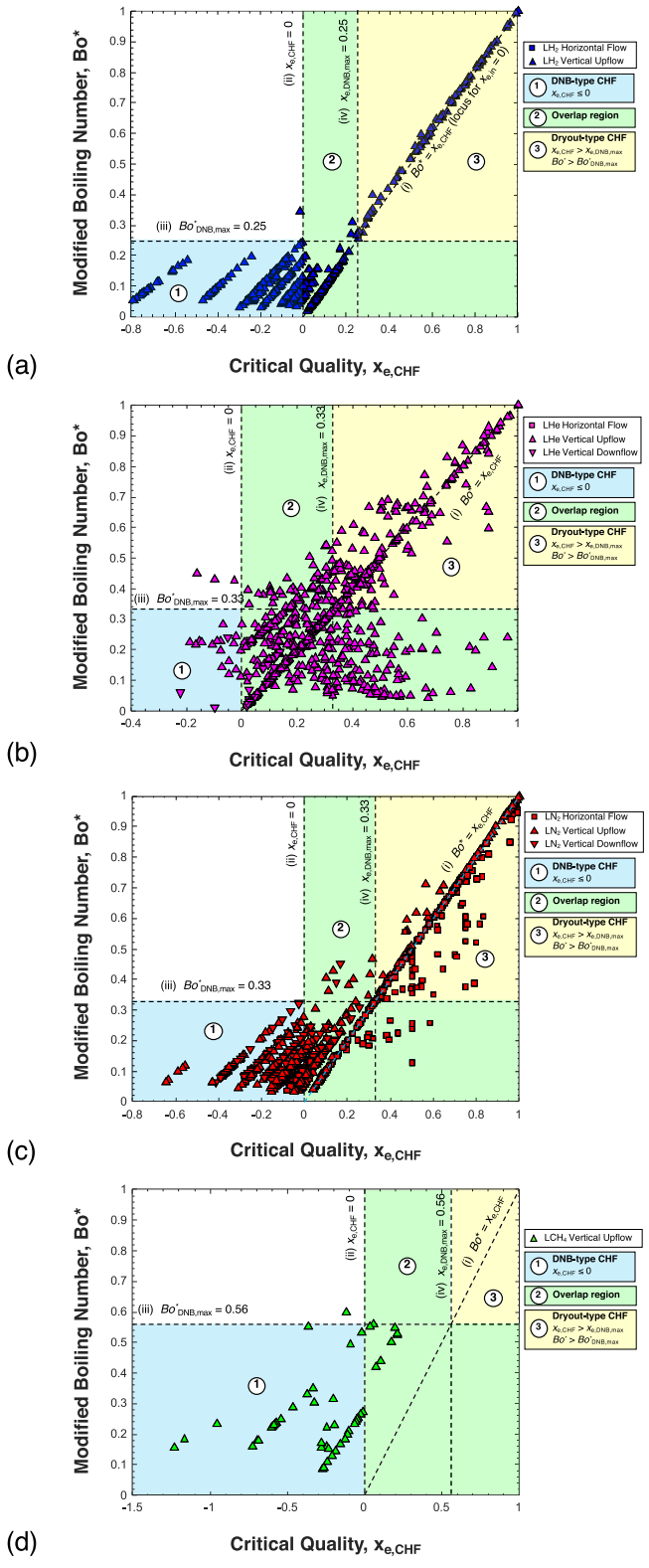

Fig. 11. Technique for distinguishing DNB-type CHF data from Dryout-type CHF data in Bo^* versus $x_{e,CHF}$ coordinates for (a) LH_2, (b) LHe, (c) LN_2, and (d) LCH_4.

the latter based on the reasoning Bo^* is lower for DNB than Dryout as mentioned earlier. A fourth demarcation line (iv), referred to as $x_{e,DNB,max}$, is the critical quality corresponding to $Bo^*_{DNB,max}$, and is found from the intersection of lines (i) and (iii). The significance of $x_{e,DNB,max}$ is that it indicates the minimum value of critical quality for Dryout. Using the four demarcation lines, two distinct regions

for DNB and Dryout can be carved out along with an overlap region.

An alternate method to separating DNB data from Dryout data is to plot modified boiling number against measured CHF; results from which are shown in Figs. 12(a)-(d) for LH_2, LHe, LN_2, and LCH_4, respectively. Here, two demarcation lines are used: (i) $Bo^*_{DNB,max}$ from Fig. 11, which signifies the maximum value of Bo exhibited by DNB data, and (ii) $q_{Dryout,max}$, which is the maximum heat flux value exhibited by Dryout data. Figure 12 shows remarkable separation of CHF data, with Dryout data exhibiting a combination of low q_{CHF} and high Bo^*, while DNB data are concentrated in a region having a combination of high q_{CHF} and low Bo^*. Here too, there is an overlap region in between. Notice that the effectiveness of separating CHF types depends largely on the number of data points for a given fluid, with LCH_4 providing the least amount of separation.

Unable to segregate data within the overlap region using the coordinates in Figs. 11 and 12, a third method is put to use in which Bo^*, is plotted against critical void fraction, α_{CHF}, as shown in Fig. 13, which is found from Zivi's relation, Eq. (12), using the critical quality, $x_{e,CHF}$. The rationale adopted here is that, unlike $x_{e,DNB,max}$, the density ratio present in the void fraction correlation, Eq. (12), would tackle differences among different fluids by providing a threshold for α_{CHF} which would demarcate the DNB data from Dryout data. Using this method, a 'conservative' DNB correlation is constructed for each fluid using the data points with $x_{e,CHF} \leq 0$ as such data are definitely associated with DNB. This conservative DNB correlation is then tested for the same fluid against all the CHF data with $x_{e,CHF} > 0$ over the entire spectrum of α_{CHF} of 0 – 1. The goal here is to identify a threshold α_{CHF} value *that is consistent for all four fluids*, where the conservative DNB correlation starts to fail by either producing unreasonably high values of mean absolute error (MAE) and root mean squared error (RMS) or show extremely low percentages of data points predicted within ±30% (θ) and ±50% (ξ). The definitions of MAE and RMS are as follows,

$$MAE = \frac{1}{N}\sum \frac{\left|q_{CHF,pred} - q_{CHF,meas}\right|}{q_{CHF,meas}} \times 100\%. \tag{20}$$

$$\text{and } RMS = \sqrt{\frac{1}{N}\sum \left(\frac{q_{CHF,pred} - q_{CHF,meas}}{q_{CHF,meas}}\right)^2} \times 100\%. \tag{21}$$

Based on the Bo^* expression in Eq. (18), a general power-law functional form is proposed to correlate the CHF data.

$$\frac{4Bo\frac{L_{CHF}}{D}}{1-x_{e,in}} = c_1 We_{fo,D}^{c_2}\left(\frac{\rho_f}{\rho_g}\right)^{c_3}(1-x_{e,in})^{c_4}\left(\frac{L_{CHF}}{D}\right)^{c_5}. \tag{22}$$

Values of both coefficient C_1 and exponents C_2 – C_5 in Eq. (22) are varied for each CHF Database classifier, *i.e.,* fluid, orientation, and CHF type. Notice that, when rearranged, Eq. (22) obeys the functional form given earlier by Eq. (6).

$$Bo = \frac{q_{CHF}}{Gh_{fg}} = 0.25c_1 We_{fo,D}^{c_2}\left(\frac{\rho_f}{\rho_g}\right)^{c_3}(1-x_{e,in})^{1+c_4}\left(\frac{L_{CHF}}{D}\right)^{c_5-1}, \tag{23}$$

which is similar to the CHF form proposed by Hall and Mudawar [101] to correlate water data,

$$Bo = \frac{q_{CHF}}{Gh_{fg}} = \tilde{c}_1 We_{fo,D}^{\tilde{c}_2}\left(\frac{\rho_f}{\rho_g}\right)^{\tilde{c}_3}\left(1-\tilde{c}_4\left(\frac{\rho_f}{\rho_g}\right)^{\tilde{c}_5}x_{e,in}\right)\left(\frac{L_{CHF}}{D}\right)^{\tilde{c}_6}, \tag{24}$$

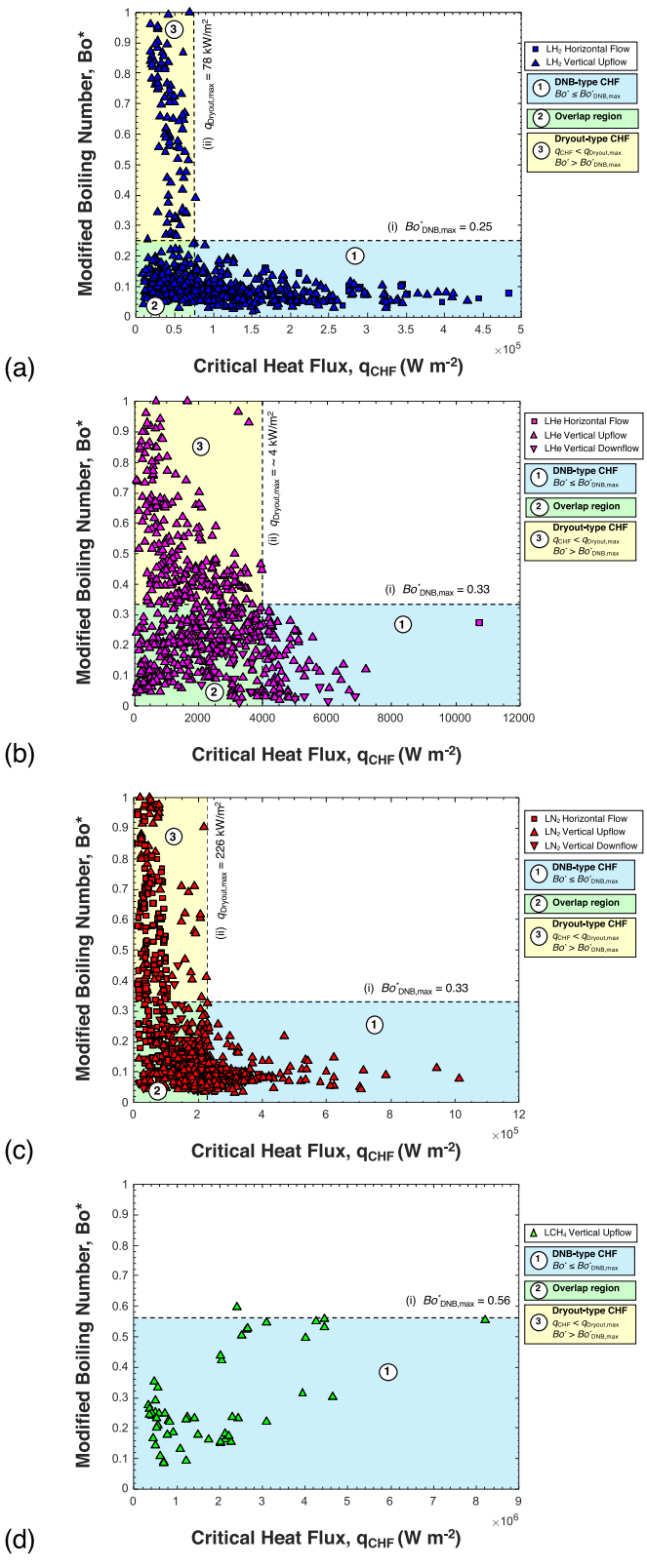

Fig. 12. Technique for distinguishing DNB-type CHF data from Dryout-type CHF data in Bo^* versus q_{CHF} coordinates for (a) LH_2, (b) LHe, (c) LN_2, and (d) LCH_4.

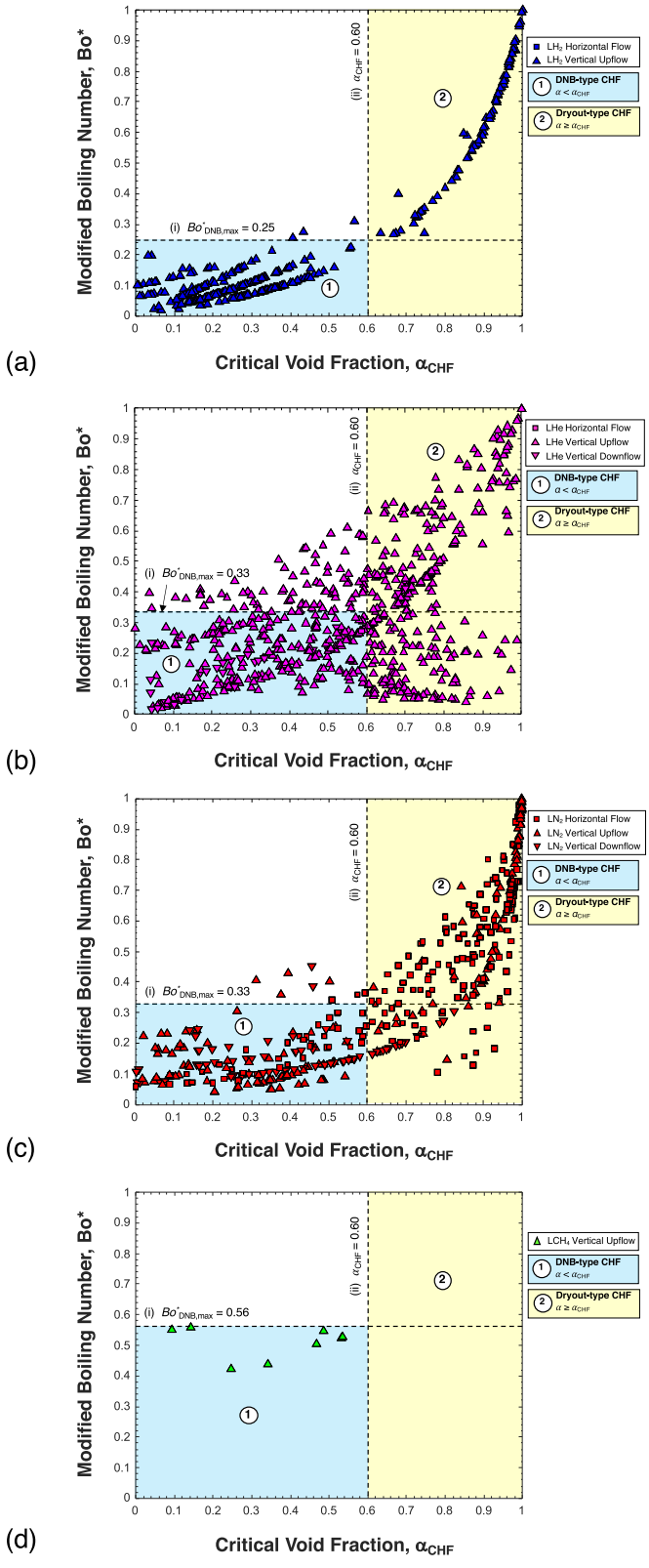

Fig. 13. Technique for distinguishing DNB-type CHF data from Dryout-type CHF data in Bo^* versus α_{CHF} coordinates for (a) LH_2, (b) LHe, (c) LN_2, and (d) LCH_4.

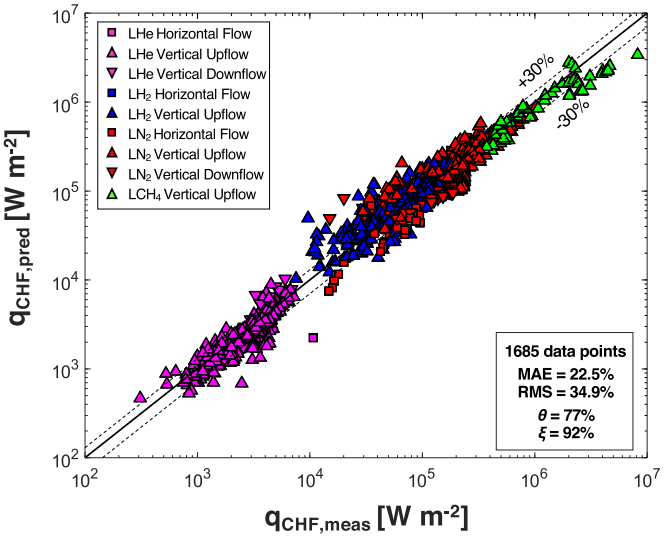

Fig. 14. Comparison of DNB data for all fluids and all flow orientations (with $\alpha_{CHF} < 0.6$) against predictions of the universal DNB correlation.

except their use of another density ratio term as multiplier to inlet quality. In this study, these two terms have been decoupled, thereby satisfying the limiting case of $q_{CHF} \to 0$ for $x_{e,in} \to 1$.

An initial step-by-step procedure is first adopted whose sole purpose is to determine a threshold value for α_{CHF} which would demarcate DNB data from Dryout data, hence paving the way for development of separate universal correlation for each CHF type. The procedure for determining the threshold value for α_{CHF} is as follows. Using Eq. (22), 'conservative' initial correlations are first attempted for DNB data for each of LH_2, LHe, LN_2, and LCH_4 individually in section 5.1(a), 5.2(a), 5.3(a) and 5.4(a), respectively, of Table 5. These correlations are deemed conservative because they correspond to only a subset of the data for each fluid corresponding to $\alpha_{CHF} = 0$, which undoubtedly correspond to DNB CHF. Subsequently, the same conservative correlations are tested in parts 5.1(b), 5.2(b), 5.3(b) and 5.4(b) of Table 5 against the remaining CHF data spanning the entire spectrum of α_{CHF}. The predictive performance of the conservative DNB correlation for each fluid is also provided in Table 5. For LH_2, the MAE and RMS are shown fluctuating until $\alpha_{CHF} = 0.5$, beyond which both appear to undergo a sharp rise. But, more evident in 5.1(b) of Table 5 is how, beyond $\alpha_{CHF} = 0.6$, none of the data are predicted within even ±50% of predictions. This clearly points to a drastic change in physics. There are two possibilities for such a drastic change: (i) change in flow orientation or (ii) change in CHF mechanism. As can be seen in Fig. 13(a), beyond $\alpha_{CHF} = 0.6$, LH_2 data are is predominantly associated with vertical upflow, therefore the drastic change is attributed to a change in CHF mechanism rather than to orientation. Hence, the threshold to demarcate DNB data from Dryout data is narrowed down to $\alpha_{CHF} = 0.5$ – 0.7 for LH_2. For LHe, similar drastic increases in MAE and RMS are observed above $\alpha_{CHF} = 0.6$. For LN_2, however, no such increases in MAE and RMS are observed, and the conservative DNB correlation works reasonably well over the entire span of α_{CHF} with fluctuating MAE and RMS. For LCH_4, there are no Dryout data and the conservative CHF correlation performs well for all the LCH_4 data. Combining these trends, it can be inferred with reasonable confidence that the threshold value of α_{CHF} for demarcating DNB data from Dryout data is 0.6. A graphical representation of this demarcation was shown earlier in Figs. 13(a)-(d).

Table 5
Conservative correlations first developed for DNB-type data for each of LH_2, LHe, LN_2, and LCH_4 separately and then tested for remaining CHF data spanning entire spectrum of critical void fraction.

5.1(a) LH_2 conservative DNB-type CHF correlation, with $x_{e,CHF} \leq 0$, developed using CHF Database with prescribed inlet and critical conditions
Application: LH_2, DNB, vertical upflow, vertical downflow
Correlation constants: $C_1 = 0.15$, $C_2 = -0.17$, $C_3 = -0.25$, $C_4 = 0.73$, $C_5 = 0.47$
Accuracy: MAE (%) = 17.6, RMS (%) = 31.0, θ (%) = 87, ξ (%) = 95
Parameter ranges

P_R [-]	D x 10^3 [m]	L_{CHF}/D [-]	P x 10^{-6} [N m^{-2}]	G [kg m^{-2} s^{-1}]	$x_{e,in}$ [-]	$\Delta P_{max}/P$ [-]	$x_{e,CHF}$ [-]	α_{CHF} [a] [-]
0.31	3	8.3	0.4	42	-0.89	0	-0.8	0
0.85	9	50	1.1	2642.9	-0.07	0.04	0	0

5.1(b) LH_2 comparison of performance of conservative DNB-type CHF correlation for LH_2 from 5.1(a) over entire spectrum of void fractions irrespective of flow orientation

Void fraction range	No. data points	MAE %	RMS %	θ %	ξ %
$\alpha_{CHF} = 0$	352	17.6	31.0	87	95
$0 < \alpha_{CHF} \leq 0.1$	25	29.5	40.6	68	76
$0.1 < \alpha_{CHF} \leq 0.2$	94	19.2	22.5	85	97
$0.2 < \alpha_{CHF} \leq 0.3$	79	21.4	31.7	80	95
$0.3 < \alpha_{CHF} \leq 0.4$	64	20.8	27.5	78	92
$0.4 < \alpha_{CHF} \leq 0.5$	20	26	31.8	60	85
$0.5 < \alpha_{CHF} \leq 0.6$	**4**	**47.8**	**50**	**25**	**25**
$0.6 < \alpha_{CHF} \leq 0.7$	**5**	**61.1**	**61.2**	**0**	**0**
$0.7 < \alpha_{CHF} \leq 0.8$	13	67.2	67.2	0	0
$0.8 < \alpha_{CHF} \leq 0.9$	21	72.7	72.7	0	0
$0.9 < \alpha_{CHF} \leq 1$	52	74.7	74.7	0	0

5.2(a) LHe conservative DNB-type CHF correlation, with $x_{e,CHF} \leq 0$, developed using CHF Database with prescribed inlet and critical conditions
Application: LHe, DNB, vertical upflow, vertical downflow
Correlation constants: $C_1 = 0.17$, $C_2 = -0.26$, $C_3 = -0.31$, $C_4 = 0.2$, $C_5 = 0.8$
Accuracy: MAE (%) = 8.6, RMS (%) = 11.9, θ (%) = 100, ξ (%) = 100
Parameter ranges

P_R [-]	D x 10^3 [m]	L_{CHF}/D [-]	P x 10^{-6} [N m^{-2}]	G [kg m^{-2} s^{-1}]	$x_{e,in}$ [-]	$\Delta P_{max}/P$ [-]	$x_{e,CHF}$ [-]	α_{CHF} [a] [-]
0.48	1	2.5	0.11	35	-1.11	0	-0.22	0
0.93	2.1	78	0.21	470	-0.11	0	0	0

5.2(b) LH_e comparison of performance of conservative DNB-type CHF correlation for LHe from 5.2(a) over entire spectrum of void fractions irrespective of flow orientation

Void fraction range	No. data points	MAE %	RMS %	θ %	ξ %
$\alpha_{CHF} = 0$	23	8.6	11.9	100	100
$0 < \alpha_{CHF} \leq 0.1$	33	17	26.5	82	88
$0.1 < \alpha_{CHF} \leq 0.2$	52	22.3	29.3	75	92
$0.2 < \alpha_{CHF} \leq 0.3$	71	24.4	30.6	70	91
$0.3 < \alpha_{CHF} \leq 0.4$	61	29.9	37.2	59	82
$0.4 < \alpha_{CHF} \leq 0.5$	72	38.1	52.8	43	74
$0.5 < \alpha_{CHF} \leq 0.6$	**83**	**73.1**	**92.1**	**25**	**40**
$0.6 < \alpha_{CHF} \leq 0.7$	**119**	**132.8**	**189.5**	**22**	**34**
$0.7 < \alpha_{CHF} \leq 0.8$	94	196	286.7	19	29
$0.8 < \alpha_{CHF} \leq 0.9$	41	226.5	327.6	10	17
$0.9 < \alpha_{CHF} \leq 1$	40	120.6	172.7	12	25

5.3(a) LN_2 conservative DNB-type CHF correlation, with $x_{e,CHF} \leq 0$, developed using CHF Database with prescribed inlet and critical conditions
Application: LN_2, DNB, vertical upflow, vertical downflow, horizontal flow
Correlation constants: $C_1 = 0.11$, $C_2 = -0.18$, $C_3 = -0.4$, $C_4 = 0.67$, $C_5 = 0.75$
Accuracy: MAE (%) = 19.1, RMS (%) = 33.8, θ (%) = 84, ξ (%) = 94
Parameter ranges

P_R [-]	D x 10^3 [m]	L_{CHF}/D [-]	P x 10^{-6} [N m^{-2}]	G [kg m^{-2} s^{-1}]	$x_{e,in}$ [-]	$\Delta P_{max}/P$ [-]	$x_{e,CHF}$ [-]	α_{CHF} [a] [-]
0.1	1.3	16.7	0.34	78.4	-0.76	-0.01	-0.65	0
0.59	12.8	230.8	2	8203.9	-0.06	0.02	0	0

5.3(b) LN_2 comparison of performance of conservative DNB-type CHF correlation for LN_2, from 5.3(a) over entire spectrum of void fractions irrespective of flow orientation

Void fraction range	No. data points	MAE %	RMS %	θ %	ξ %
$\alpha_{CHF} = 0$	411	19.1	33.8	84	94
$0 < \alpha_{CHF} \leq 0.1$	26	30	33.4	58	92
$0.1 < \alpha_{CHF} \leq 0.2$	27	28.5	32.9	55	93
$0.2 < \alpha_{CHF} \leq 0.3$	28	32	39.8	36	86
$0.3 < \alpha_{CHF} \leq 0.4$	36	46.5	62.7	39	75
$0.4 < \alpha_{CHF} \leq 0.5$	36	32.2	36.6	39	92
$0.5 < \alpha_{CHF} \leq 0.6$	**35**	**41.8**	**43.9**	**26**	**63**
$0.6 < \alpha_{CHF} \leq 0.7$	**31**	**48.7**	**50**	**10**	**42**
$0.7 < \alpha_{CHF} \leq 0.8$	34	55	55.7	0	26
$0.8 < \alpha_{CHF} \leq 0.9$	50	59.2	61.6	6	12
$0.9 < \alpha_{CHF} \leq 1$	127	48.7	56.1	30	44

(*continued on next page*)

Table 5
(*continued*)

5.4(a) LCH_4 conservative DNB-type CHF correlation, with $x_{e,CHF} \leq 0$, developed using CHF Database with prescribed inlet and critical conditions
Application: LCH_4, DNB, vertical upflow
Correlation constants: $C_1 = 0.21$, $C_2 = -0.21$, $C_3 = -0.42$, $C_4 = 0.14$, $C_5 = 0.73$
Accuracy: MAE (%) = 14.6, RMS (%) = 21.4, θ (%) = 87, ξ (%) = 98
Parameter ranges

P_R [-]	D x 10^3 [m]	L_{CHF}/D [-]	P x 10^{-6} [N m^{-2}]	G [kg m^{-2} s^{-1}]	$x_{e,in}$ [-]	$\Delta P_{max}/P$ [-]	$x_{e,CHF}$ [-]	α_{CHF} [a] [-]
0.22	1.4	18.1	1.03	225.8	-2.06	0	-1.23	0
0.89	8.5	98.5	4.07	7017	-0.38	0.03	-0.01	0

5.4(b) LCH_4 comparison of performance of conservative DNB-type CHF correlation for LCH_4 from 5.4(a) over entire spectrum of void fractions irrespective of flow orientation

Void fraction range	No. data points	MAE %	RMS %	θ %	ξ %
$\alpha_{CHF} = 0$	45	14.6	21.4	87	98
$0 < \alpha_{CHF} \leq 0.6$	8	37.9	38.7	25	100

[a] Evaluated using Zivi's void fraction, Eq. (12). Test cases with $\alpha_{CHF} = 0$ signify occurrence of DNB-type CHF.

Table 6
Universal DNB correlation for cryogens developed using data for all four fluids and all flow orientations with $\alpha_{CHF} < 0.6$.

Application: LH_2, LHe, LN_2, LCH_4, vertical upflow, vertical downflow, horizontal flow
Correlation constants: $C_1 = 0.17$, $C_2 = -0.21$, $C_3 = -0.32$, $C_4 = 1.07$, $C_5 = 0.59$
Accuracy: MAE (%) = 22.5, RMS (%) = 34.9, θ (%) = 77, ξ (%) = 92
Parameter ranges

P_R [-]	D x 10^3 [m]	L_{CHF}/D [-]	P x 10^{-6} [N m^{-2}]	G [kg m^{-2} s^{-1}]	$x_{e,in}$ [-]	$\Delta P_{max}/P$ [-]	$x_{e,CHF}$ [-]	α_{CHF} [a] [-]
0.1	0.5	2.5	0.08	4.2	-2.06	-0.01	-1.23	0
0.93	14.1	230.8	4.07	8203.9	0.28	0.17	0.44	0.6

[a] Evaluated using Zivi's void fraction Eq. (12).

Table 7
Universal Dryout correlation for cryogens developed using data for all four fluids with $\alpha_{CHF} \geq 0.6$.

7(a) Correlation of Dryout data for all orientations combined
Application: LH_2, LHe, LN_2, LCH_4, vertical upflow, vertical downflow, horizontal flow
Correlation constants: $C_1 = 0.9$, $C_2 = -0.22$, $C_3 = -0.19$, $C_4 = 1.68$, $C_5 = 0.21$
Accuracy: MAE (%) = 28.7, RMS (%) = 40.5, θ (%) = 65, ξ (%) = 84
Parameter ranges

P_R [-]	D x 10^3 [m]	L_{CHF}/D [-]	P x 10^{-6} [N m^{-2}]	G [kg m^{-2} s^{-1}]	$x_{e,in}$ [-]	$\Delta P_{max}/P$ [-]	$x_{e,CHF}$ [-]	α_{CHF} [a] [-]
0.03	0.5	3	0.01	2.2	-0.62	0	0.1	0.6
0.9	14.1	226.3	3.06	680	0.95	0.17	1	1

7(b) Correlation of Dryout data for horizontal flow
Application: LH_2, LHe, LN_2, LCH_4, horizontal flow
Correlation constants: $C_1 = 1.1$, $C_2 = -0.25$, $C_3 = -0.28$, $C_4 = -0.6$, $C_5 = 0.29$
Accuracy: MAE (%) = 20.1, RMS (%) = 27.6, θ (%) = 78, ξ (%) = 97
Parameter ranges

P_R [-]	D x 10^3 [m]	L_{CHF}/D [-]	P x 10^{-6} [N m^{-2}]	G [kg m^{-2} s^{-1}]	$x_{e,in}$ [-]	$\Delta P_{max}/P$ [-]	$x_{e,CHF}$ [-]	α_{CHF} [a] [-]
0.03	2.9	11.3	0.11	44	-0.2	0	0.11	0.61
0.9	14	205	3.06	470	0.86	0.14	0.99	1

7(c) Correlation of Dryout data for vertical upflow and vertical downflow
Application: LH_2, LHe, LN_2, LCH_4, vertical upflow, vertical downflow
Correlation constants: $C_1 = 0.85$, $C_2 = -0.22$, $C_3 = -0.22$, $C_4 = 1.83$, $C_5 = 0.22$
Accuracy: MAE (%) = 26.1, RMS (%) = 36.8, θ (%) = 70, ξ (%) = 89
Parameter ranges

P_R [-]	D x 10^3 [m]	L_{CHF}/D [-]	P x 10^{-6} [N m^{-2}]	G [kg m^{-2} s^{-1}]	$x_{e,in}$ [-]	$\Delta P_{max}/P$ [-]	$x_{e,CHF}$ [-]	α_{CHF} [a] [-]
0.03	0.5	3	0.01	2.2	-0.62	0	0.1	0.6
0.87	14.1	226.3	1.65	680	0.95	0.17	1	1

[a] Evaluated using Zivi's void fraction Eq. (12).

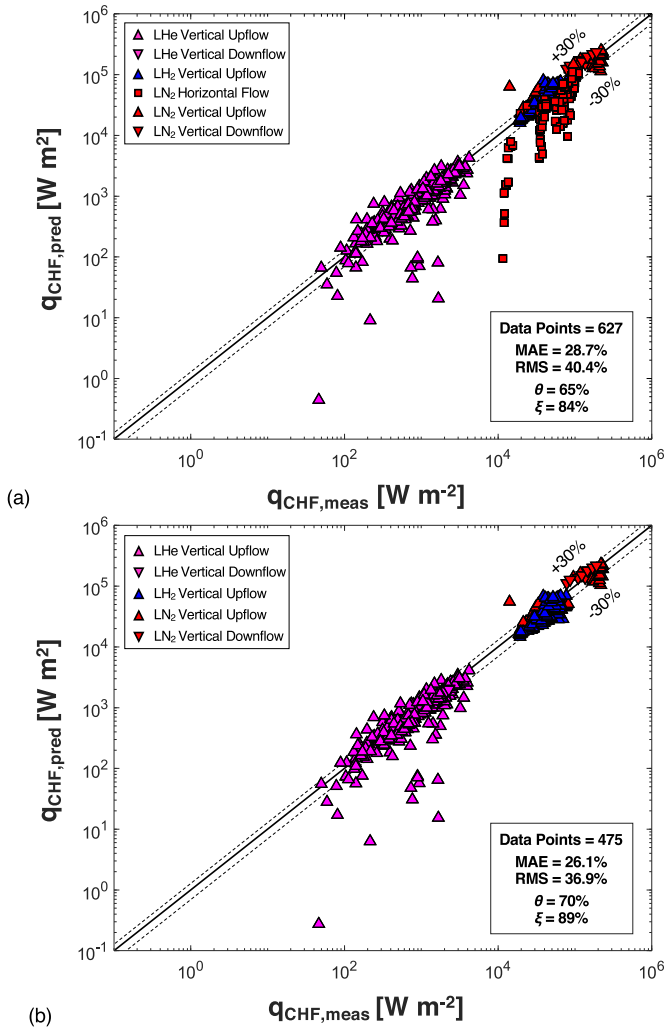

Fig. 15. Comparison of Dryout data (with $\alpha_{CHF} \geq 0.6$) against predictions of universal Dryout correlations for all fluids and (a) all flow orientations and (b) only vertical upflow and vertical downflow.

5.2. Universal Correlations for DNB and Dryout

5.2.1. Universal DNB correlation

Using the threshold value for α_{CHF} from above and the functional form in Eq. (22), a universal DNB correlation is developed by now considering data *for all four fluids* with $\alpha_{CHF} < 0.6$.

$$\frac{4Bo\frac{L_{CHF}}{D}}{1-x_{e,in}} = 0.17We_{fo,D}^{-0.21}\left(\frac{\rho_f}{\rho_g}\right)^{-0.32}(1-x_{e,in})^{1.07}\left(\frac{L_{CHF}}{D}\right)^{0.59}. \quad (25)$$

The performance of the universal correlation is detailed in Table 6 and illustrated graphically in Fig. 14. With a MAE of 22.5% *irrespective of fluid or flow orientation*, this correlation provides very good agreement with the data. The coefficient and exponents in Eq. (25) were found using the genetic algorithm-based optimization tool in the MATLAB Global Optimization Toolbox [102] which iteratively varies both the coefficient and exponents to find the global minimum as opposed to local minimum. The error which is chosen to be minimized is the MAE, Eq. (20).

5.2.2. Universal Dryout correlation

Similarly, using the MATLAB Global Optimization Toolbox [102], a universal correlation for the Dryout data ($\alpha_{CHF} \geq 0.6$) is developed for *all four fluids and all orientations*,

$$\frac{4Bo\frac{L_{CHF}}{D}}{1-x_{e,in}} = 0.9We_{fo,D}^{-0.22}\left(\frac{\rho_f}{\rho_g}\right)^{-0.19}(1-x_{e,in})^{1.68}\left(\frac{L_{CHF}}{D}\right)^{0.21}. \quad (26)$$

The performance of this correlation is detailed in part 7(a) of Table 7 and illustrated graphically in Fig. 15(a). With a MAE of 28.7% *irrespective of fluid or flow orientation*, this correlation also provides good agreement with the data, with an exception of few LN_2 data points. These LN_2 data points are associated with horizontal flow data and available from Steiner and Schlünder [67] and Müller *et al.* [93], who employed the same test section. Müller *et al.* [93] reported that CHF was mainly influenced by system pressure and flow quality, and the influence of mass velocity on CHF was rather small. Since flow boiling CHF data throughout the literature are strongly correlated to $We_{fo,D}$, which, in turn, is proportional to G^2, deviation of the LN_2 data from Müller *et al.* are not readily explainable. Nonetheless, these deviations appear to be responsible for the data departure observed in Fig. 15(a). Additionally, the departure of a few LHe data points in Fig. 15(a) might be attributed, as discussed earlier, to the high measurement errors associated with this particular cryogen at extreme low temperatures. Departure of these LHe data points from the majority of LHe data (including similar operating conditions) appears to point to much higher measurement inaccuracies for these specific data points.

Further examination of the CHF Database showed more pronounced flow orientation effects on CHF for the Dryout data compared to relatively insignificant for the DNB data as discussed in the previous section. This is particularly the case for LN_2 horizontal flow data [67,93] corresponding to values of modified Froude number, Fr^*, below 1.7. In fact, slightly better predictions are observed by constructing a Dryout correlation for horizontal flow, Table 7(b), separate from that for vertical upflow and vertical downflow combined, Table 7(c). Figure 15(b) shows the performance of the Dryout correlation for combined vertical upflow and vertical downflow.

5.2.3. Comparative predictions with previous CHF correlations

Table 8 compares predictive accuracy of the present correlations with those of prior correlations available for a multitude of fluids, some including cryogens. The following prior correlations are examined: (1) Hall and Mudawar's [22] inlet and outlet based subcooled DNB-type correlations, (2) Shah's [103] universal correlation for both DNB and Dryout, and (3) Katto and Ohno's [23] seminal correlation for both DNB and Dryout.

For the DNB data, Table 8 shows Hall and Mudawar's inlet-based subcooled CHF correlation provides good predictions of the cryogen data, followed in turn by Hall and Mudawar's outlet-based correlation, Shah's correlation, and Katto and Ohno's correlation, with the latter showing lowest predictive accuracy. Interestingly, both the Shah and the Katto and Ohno correlations were constructed using some cryogen data.

For the Dryout data, Table 8 shows Shah's correlation provides reasonable results, but that of Katto and Ohno shows appreciable scatter.

Table 8 also shows how the present correlations, developed specifically for cryogens, while providing somewhat similar predictions for upflow DNB as Hall and Mudawar's inlet-based correlation, is superior in terms of overall agreement for both vertical and horizontals flows. The present correlation also provides significant improvements over the Shah and the Katto and Ohno correlations. As to Dryout predictions, the present correlations provides predictions somewhat comparable to those of Shah but far more superior than those of Katto and Ohno. Overall, the present correlations for both DNB and Dryout CHF provide very good predictions consistently for both vertical and horizontal flows.

Table 8
Performance of existing CHF correlations against the PU-BTPFL Cryogen Flow Boiling CHF Database.

Author(s)	Equation(s)	Remarks	1685 DNB type CHF data points ($\alpha_{CHF} < 0.6$)				627 Dryout type CHF data points ($\alpha_{CHF} \geq 0.6$)			
			Vertical Flows		Horizontal Flow		Vertical Flows		Horizontal Flow	
			MAE (%)	RMS (%)	MAE (%)	RMS (%)	MAE (%)	RMS (%)	MAE (%)	RMS (%)
Hall & Mudawar [22] (Outlet)	$\frac{q_{CHF}}{Gh_{fg}} = c_1 We_{fo,D}^{c_2}\left(\frac{\rho_f}{\rho_g}\right)^{c_3}\left[1 - c_4\left(\frac{\rho_f}{\rho_g}\right)^{c_5} x_{e,CHF}\right]$ $c_1 = 0.0722$, $c_2 = -0.312$, $c_3 = -0.644$, $c_4 = 0.9$, $c_5 = 0.724$	5544 data points Fluid(s): H_2O CHF Type: DNB Vertical and Horizontal Flows	37.7	68.9	44.7	68.9				
Hall & Mudawar[a] [22] (Inlet)	$\frac{q_{CHF}}{Gh_{fg}} = \frac{c_1 We_{fo,D}^{c_2}\left(\frac{\rho_f}{\rho_g}\right)^{c_3}\left[1 - c_4\left(\frac{\rho_f}{\rho_g}\right)^{c_5} x_{e,in*}\right]}{1 + 4c_1c_4 We_{fo,D}^{c_2}\left(\frac{\rho_f}{\rho_g}\right)^{c_3+c_5}\left(\frac{L_{CHF}}{D}\right)}$ $c_1 = 0.0722$, $c_2 = -0.312$, $c_3 = -0.644$, $c_4 = 0.9$, $c_5 = 0.724$		21.0	32.7	26.2	35.2			
Shah [103]	Calculate $x_{e,CHF}$: Evaluate Shah's correlation parameter: $Y = \left[\frac{GDc_{p,f}}{k_f}\right]\left[\frac{G^2}{\rho_f^2 gD}\right]^{0.4}\left[\frac{\mu_f}{\mu_g}\right]^{0.6}$ For LHe, use Upstream Conditions Correlation ($q_{CHF,UCC}$). For all other fluids: if $Y \leq 10^6$, $q_{CHF} = q_{CHF,UCC}$ if $Y > 10^6$ and $L_E > \frac{160}{P_R^{1.14}}$, $q_{CHF} = q_{CHF,UCC}$ if $Y > 10^6$ and $L_E \leq \frac{160}{P_R^{1.14}}$, $q_{CHF} = \min(q_{CHF,UCC}, q_{CHF,LCC})$, where $q_{CHF,LCC}$ is the Local Conditions Correlation. Upstream Conditions Correlation: $\frac{q_{CHF,UCC}}{Gh_{fg}} = 0.124(\frac{D}{L_E})^{0.89}(\frac{10^4}{Y})^n(1 - x_{e,in,E})$ Where, if $x_{e,in} \leq 0$, $L_E = L_{CHF}$, $x_{e,in,E} = x_{e,in}$ if $x_{e,in} > 0$, $L_E = L_B$, $x_{e,in,E} = 0$ and, $\frac{L_B}{D} = \frac{x_{e,CHF}}{4Bo} = \frac{L_{CHF}}{D} + \frac{x_{e,in}}{4Bo}$ For LHe, $n = (\frac{D}{L_E})^{0.33}$ For all other fluids: if $Y \leq 10^4$, $n = 0$ if $Y > 10^4$ and $Y \leq 10^6$, $n = (\frac{D}{L_E})^{0.54}$ if $Y > 10^6$, $n = \frac{0.12}{(1 - x_{e,in,E})^{0.5}}$ Local Conditions Correlation: $\frac{q_{CHF,LCC}}{Gh_{fg}} = F_E F_x Bo_{x_{e,CHF}=0}$ Where, $F_E = \max\{1, (1.54 - 0.032(\frac{L_{CHF}}{D}))\}$ $Bo_{x_{e,CHF}=0} = \max\{\frac{15Y^{-0.612}}{0.0024Y^{-0.105}(1 + 1.15P_R^{3.39})}\}$ For $x_{e,CHF} > 0$, $F_x = F_3[1 + \frac{(F_3^{-0.29} - 1)(P_R - 0.6)}{0.35}]^c$ if $P_R \leq 0.6$, $c = 0$ if $P_R > 0.6$, $c = 1$ $F_3 = \left(\frac{1.25 \times 10^5}{Y}\right)^{0.833 x_{e,CHF}}$ For $x_{e,CHF} < 0$, $F_x = F_1\left[1 - \frac{(1 - F_2)(P_R - 0.6)}{0.35}\right]^b$ if $P_R \leq 0.6$, $b = 0$ if $P_R > 0.6$, $b = 1$ $F_1 = 1 + 0.0052(-x_{e,CHF}^{0.88})(\min\{1.4 \times 10^7, Y\})^{0.41}$ if $F_1 \leq 4$, $F_2 = F_1^{-0.42}$ if $F_1 > 4$, $F_2 = 0.55$	1443 data points Fluid(s): H_2O, R-11, R-12, R-21, R-22, R-113, R-114, LHe, LH_2, LN_2, Ammonia, Hydrazine, Acetone, Benzene, Diphenyl, Ethanol, Ethylene Glycol, N_2O_4, CO_2 CHF Type: DNB and Dryout Vertical Upflow	48.9	95	98.4	141.9	27.7	43.5	20.6	28.3

(continued on next page)

Table 8 (*continued*)

Author(s)	Equation(s)	Remarks	1685 DNB type CHF data points ($\alpha_{CHF} < 0.6$)				627 Dryout type CHF data points ($\alpha_{CHF} \geq 0.6$)			
			Vertical Flows		Horizontal Flow		Vertical Flows		Horizontal Flow	
			MAE (%)	RMS (%)	MAE (%)	RMS (%)	MAE (%)	RMS (%)	MAE (%)	RMS (%)
Katto & Ohno [23]	$\frac{q_{CHF}}{Gh_{fg}} = \frac{q_{CHF,x_{e,in}=0}}{Gh_{fg}}(1 - Kx_{e,in})$ if $\frac{\rho_g}{\rho_f} < 0.15$, if $q_{co,2} < q_{co,3}$, $q_{CHF,x_{e,in}=0} = q_{co,2}$ if $q_{co,2} > q_{co,3}$, if $q_{co,3} < q_{co,4}$, $q_{CHF,x_{e,in}=0} = q_{co,3}$ if $q_{co,3} > q_{co,4}$, $q_{CHF,x_{e,in}=0} = q_{co,4}$ if $K_6 > K_7$, $K = K_6$ if $K_6 < K_7$, $K = K_7$ Where, $\frac{q_{co,2}}{Gh_{fg}} = C\left(\frac{\sigma\rho_f}{G^2L_H}\right)^{0.043}\frac{1}{(L_H/D)}$ $\frac{q_{co,3}}{Gh_{fg}} = 0.1\left(\frac{\rho_g}{\rho_f}\right)^{0.133}\left(\frac{\sigma\rho_f}{G^2L_H}\right)^{1/3}\frac{1}{1+0.0031(L_H/D)}$ $\frac{q_{co,4}}{Gh_{fg}} = 0.098\left(\frac{\rho_g}{\rho_f}\right)^{0.133}\left(\frac{\sigma\rho_f}{G^2L_H}\right)^{0.433}\frac{(L_H/D)^{0.27}}{1+0.0031(L_H/D)}$ $K_6 = \frac{1.043}{4C\left(\frac{\sigma\rho_f}{G^2L_H}\right)^{0.043}}$ $K_7 = \frac{5}{6}\left[\frac{0.0124 + (D/L_H)}{(\frac{\rho_g}{\rho_f})^{0.133}(\frac{\sigma\rho_f}{G^2L_H})^{1/3}}\right]$ if $L_H/D < 50$, $C = 0.25$ if $50 \leq L_H/D \leq 150$, $C = 0.25 + 0.0009\{(L_H/D) - 50\}$ if $L_H/D > 50$, $C = 0.34$ if $\frac{\rho_g}{\rho_f} > 0.15$, if $q_{co,2} < q_{co,13}$, $q_{CHF,x_{e,in}=0} = q_{co,2}$ if $q_{co,2} > q_{co,13}$, if $q_{co,13} > q_{co,5}$, $q_{CHF,x_{e,in}=0} = q_{co,13}$ if $q_{co,13} < q_{co,5}$, $q_{CHF,x_{e,in}=0} = q_{co,5}$ if $K_6 > K_7$, $K = K_6$ if $K_6 < K_7$, if $K_7 < K_9$, $K = K_7$ if $K_9 < K_7$, $K = K_9$ Where, $\frac{q_{co,5}}{Gh_{fg}} =$ $0.0384(\frac{\rho_g}{\rho_f})^{0.6}(\frac{\sigma\rho_f}{G^2L_H})^{0.173} \times \frac{1}{1+0.28(\frac{\sigma\rho_f}{G^2L_H})^{0.233}(L_H/D)}$ $\frac{q_{co,13}}{Gh_{fg}} = 0.234(\frac{\rho_g}{\rho_f})^{0.513}(\frac{\sigma\rho_f}{G^2L_H})^{0.433}\frac{(L_H/D)^{0.27}}{1+0.0031(L_H/D)}$ $K_9 = 1.12[\frac{1.52(\frac{\sigma\rho_f}{G^2L_H})^{0.233} + (D/L_H)}{(\frac{\rho_g}{\rho_f})^{0.6}(\frac{\sigma\rho_f}{G^2L_H})^{0.173}}]$	Fluid(s): H_2O, LHe, R-12, R-22, R-115 CHF Type: DNB and Dryout Vertical Upflow	53.7	89.4	98.1	141.3	58.1	137.5	36.6	46.5
Present Study	$\frac{4Bo\frac{L_{CHF}}{D}}{1-x_{e,in}} = c_1We_{fo,D}^{c_2}(\frac{\rho_f}{\rho_g})^{c_3}(1-x_{e,in})^{c_4}(\frac{L_{CHF}}{D})^{c_5}$ DNB Type Vertical Flows: $c_1 = 0.19$, $c_2 = -0.22$, $c_3 = -0.29$, $c_4 = 1.11$, $c_5 = 0.57$ DNB Type Horizontal Flows: $c_1 = 0.32$, $c_2 = -0.24$, $c_3 = -0.60$, $c_4 = 0.48$, $c_5 = 0.69$ Dryout Type Vertical Flows (see Table 7(c)): $c_1 = 0.85$, $c_2 = -0.22$, $c_3 = -0.22$, $c_4 = 1.83$, $c_5 = 0.22$ Dryout Type Horizontal Flows (see Table 7(b)): $c_1 = 1.1$, $c_2 = -0.25$, $c_3 = -0.28$, $c_4 = -0.6$, $c_5 = 0.29$	2312 data points Fluid(s): LH_2, LHe, LN_2 and LCH_4, CHF Type: DNB and Dryout Vertical and Horizontal Flows	21.9	36.5	16.5	21.7	26.1	36.8	20.1	27.6

[a] Under constant pressure assumption, $x_{e,in^*} = x_{e,in}$

6. Conclusions and Recommendations

The present study was motivated by the absence of a large, reliable, error-free CHF database for developing and validating CHF correlations as well as future analytic and computational models. An exhaustive literature search identified nearly 50 useful individual CHF databases for four different fluids, LH_2, LHe, LN_2, and LCH_4, and acceptable data were consolidated into a single PU-BTPFL Cryogen Flow Boiling CHF database – CHF Database for short. An exhaustive parametric study of the Database was performed to gain insight into the fluid physics unique to cryogens, and to aid future investigators into important operating conditions where there is a dearth of data. Finally, using the Database, universal CHF correlations are constructed for two distinct CHF mechanisms, DNB and Dryout, which required careful physics-based segregation of the data. The new CHF correlations, intended specifically for cryogens, were found to provide good agreement with the data in terms of both predictive accuracy and trends.

A detailed assessment of the CHF Database illuminated key oversights researchers sometimes make when performing cryogen experiments. The present authors propose the following strategy for acquiring useful CHF data:

1 Local wall temperatures should be measured along the flow direction using temperature sensors to determine local heat transfer characteristics. Methods such as using a Wheatstone Bridge to find average wall temperature with respect to a reference bath temperature can strongly jeopardize both quality and accuracy of the data.
2 Inlet and outlet pressure should both be measured as close as possible to the inlet and outlet, respectively, of the heated length. Further, where a pressure drop model is employed to calculate outlet (or inlet) pressure from an upstream (or downstream) measurement, details of the model should be provided.
3 Both inlet temperature and either outlet quality or subcooling should be tabulated. The outlet conditions must be calculated from an energy balance based on fluid enthalpy (not specific heat, which varies with pressure).

Declaration of Competing Interest

NONE The authors declare that they have no known competing financial interests or personal relationships that could have appeared to influence the work reported in this paper.

Acknowledgements

The authors are grateful for financial support provided by the National Aeronautics and Space Administration (NASA) under grant no. 80GRC018C0055. The authors would also like to acknowledge the services provided by Purdue Libraries, especially its Interlibrary Loan (ILL) service, for helping acquire literature from across the world.

References

[1] E.W. Lemmon, I.H. Bell, M.L. Huber, M.O. McLinden, NIST standard reference database 23: Reference fluid thermodynamic and transport properties-REFPROP, version 10.0, Standard Reference Data Program, National Institute of Standards and Technology, Gaithersburg, 2018.
[2] D.D. Hall, I. Mudawar, Critical heat flux (CHF) for water flow in tubes – I. Compilation and assessment of world CHF data, Int. J. Heat Mass Transfer 43 (2000) 2573–3604.
[3] I. Mudawar, Recent advances in high-flux, two-phase thermal management, J. Thermal Sci. Engng Applications 5 (2013) 021012.
[4] I. Mudawar, T.M. Anderson, Parametric investigation into the effects of pressure, subcooling, surface augmentation and choice of coolant on pool boiling in the design of cooling system for high-power-density electronic chips, J. Electronic Packaging 112 (1990) 375–382.
[5] I. Mudawar, T.M. Anderson, Optimization of extended surfaces for high flux chip cooling by pool boiling, J. Electronic Packaging 115 (1993) 89–100.
[6] G. Liang, I. Mudawar, Pool boiling critical heat flux (CHF) – Part 1: Review of mechanisms, models, and correlations, Int. J. Heat Mass Transfer 117 (2018) 1352–1367.
[7] G. Liang, I. Mudawar, Review of pool boiling enhancement by surface modification, Int. J. Heat Mass Transfer 128 (2019) 892–933.
[8] J.A. Shmerler, I. Mudawar, Local evaporative heat transfer coefficient in turbulent free-falling liquid films, Int. J. Heat Mass Transfer 31 (1988) 731–742.
[9] T.H. Lyu, I. Mudawar, Statistical investigation of the relationship between interfacial waviness and sensible heat transfer to a falling liquid film, Int. J. Heat Mass Transfer 34 (1991) 1451–1464.
[10] I. Mudawar, R.A. Houpt, Measurement of mass and momentum transport in wavy-laminar falling liquid films, Int. J. Heat Mass Transfer 36 (1993) 4151–4162.
[11] D. Maddox, I. Mudawar, Single- and two-phase convective heat transfer from smooth and enhanced microelectronic heat sources in a rectangular channel, J. Heat Transfer 111 (1989) 1045–1052.
[12] T.C. Willingham, I. Mudawar, Forced-convection boiling and critical heat flux from a linear array of discrete heat sources, Int. J. Heat Mass Transfer 35 (1992) 2879–2890.
[13] C.O. Gersey, I. Mudawar, Effects of heater length and orientation on the trigger mechanism for near-saturated flow boiling CHF - I. Photographic and statistical characterization of the near-wall interfacial features, Int. J. Heat Mass Transfer 38 (1995) 629–642.
[14] J.C. Sturgis, I. Mudawar, Critical heat flux in a long, rectangular channel subjected to one-sided heating - II. Analysis of CHF data, Int. J. Heat Mass Transfer 42 (1999) 1849–1862.
[15] S. Mukherjee, I. Mudawar, Smart, low-cost, pumpless loop for micro-channel electronic cooling using flat and enhanced surfaces, in: Proc. I-Therm 2002: Int. Conf. Thermal, Mechanics and Thermomechanical Phenomena in Electronic Systems, 2002, San Diego, California, 2002, pp. 360–370. May 29-June 1.
[16] S.M. Kim, I. Mudawar, Review of databases and predictive methods for pressure drop in adiabatic, condensing and boiling mini/micro-channel flows, Int. J. Heat Mass Transfer 77 (2014) 74–97.
[17] D.C. Wadsworth, I. Mudawar, Enhancement of single-phase heat transfer and critical heat flux from an ultra-high-flux simulated microelectronic heat source to a rectangular impinging jet of dielectric liquid, J. Heat Transfer 114 (1992) 764–768.
[18] M.E. Johns, I. Mudawar, An ultra-high power two-phase jet-impingement avionic clamshell module, J. Electronic Packaging 118 (1996) 264–270.
[19] W.P. Klinzing, J. Rozzi, I. Mudawar, Film and transition boiling correlations for quenching of hot surfaces with water sprays, J. Heat Treating 9 (1992) (1992) 91–103.
[20] G. Liang, I. Mudawar, Review of spray cooling – Part 2: High temperature boiling regimes and quenching applications, Int. J. Heat Mass Transfer 115 (2017) 1206–1222.
[21] I. Mudawar, M.B. Bowers, Ultra-high critical heat flux (CHF) for subcooled water flow boiling – I: CHF data and parametric effects for small diameter tubes, Int. J. Heat Mass Transfer 42 (1999) 1405–1428.
[22] D.D. Hall, I. Mudawar, Critical heat flux (CHF) for water flow in tubes – II. Subcooled CHF correlations, Int. J. Heat Mass Transfer 43 (2000) 2605–2640.
[23] Y. Katto, H. Ohno, An improved version of the generalized correlation of critical heat flux for the forced convective boiling in uniformly heated vertical tubes, Int. J. Heat Mass Transfer 27 (1984) 1641–1648.
[24] J.W. Hartwig, A. Asensio, S.R. Darr, Assessment of Existing Two Phase Heat Transfer Coefficient and Critical Heat Flux on Cryogenic Flow Boiling Quenching Experiments, Int. J. Heat Mass Transfer 93 (2016) 441–463.
[25] M. Mercado, N. Wong, J.W. Hartwig, Assessment of Two-Phase Heat Transfer Coefficient and Critical Heat Flux Correlations for Cryogenic Flow Boiling in Pipe Heating Experiments, Int. J. Heat Mass Transfer 133 (2019) 295–315.
[26] H. Zhang, I. Mudawar, M.M. Hasan, Experimental and theoretical study of orientation effects on flow boiling CHF, Int. J. Heat Mass Transfer 45 (2002) 4463–4478.
[27] H. Zhang, I. Mudawar, M.M. Hasan, Flow boiling CHF in microgravity, Int. J. Heat Mass Transfer 48 (2005) 3107–3118.
[28] S.M. Kim, I. Mudawar, Theoretical model for annular flow condensation in rectangular micro-channels, Int. J. Heat Mass Transfer 55 (2012) 958–970.
[29] C. Konishi, I. Mudawar, Review of flow boiling and critical heat flux in microgravity, Int. J. Heat Mass Transfer 80 (2015) 469–493.
[30] H. Lee, C.R. Kharangate, N. Mascarenhas, I. Park., I. Mudawar, Experimental and computational investigation of vertical downflow condensation, Int. J. Heat Mass Transfer 85 (2015) 865–879.
[31] J. Lee, L.E. O'Neill, I. Mudawar, 3-D computational investigation and experimental validation of effect of shear-lift on two-phase flow and heat transfer characteristics of highly subcooled flow boiling in vertical upflow, Int. J. Heat Mass Transfer 150 (2020) 119291.
[32] S.M. Kim, I. Mudawar, Universal approach to predicting saturated flow boiling heat transfer in mini/micro-channels part I. Dryout incipience quality, Int. J. Heat Mass Transfer 64 (2013) 1226–1238.
[33] L.E. Dean, L.M. Thompson, K.R. Stehling, T.F. Reinhardt, W.M. Smith, Heat transfer characteristics of liquid nitrogen, Bell Aircraft Corporation, Report No. 56-982-035, 1955.
[34] H.H. Walters, Single-tube heat transfer tests with liquid hydrogen, Adv. Cryog. Eng. 6 (1961) 509–516.

[35] S. Lehongre, J.C. Boissin, C. Johannès, A. De La Harpe, Critical nucleate boiling of liquid helium in narrow tubes and annuli, in: Proc. 2nd Int. Cryo. Eng. Conf., 1968, pp. 274–275.
[36] M. Jergel, R. Stevenson, Heat transfer to liquid helium in narrow channels with laminar and turbulent flow, Appl. Phys. Lett. 17 (1970) 125–127.
[37] M. Jergel, K. Hechler, R. Stevenson, The effect of forced circulation on heat transfer with liquid helium in narrow channels, Cryogenics 10 (1970) 413–417.
[38] M. Jergel, I. Hlasnik, A few remarks on the heat transfer in helium liquid—gas flow, Cryogenics 13 (1973) 676–678.
[39] V.A. Grigoriev, Yu.M. Pavlov, E.V. Ametistov, V.I. Antipov, Heat transfer in boiling helium to superconducting elements in power generating equipment, Future energy production systems, Heat and mass transfer processes I (1976).
[40] V.I. Subbotin, V.I. Deev, V.V. Solodovnikov, V.V. Arkhipov, Heat transfer in two-phase flow of helium, Int. Heat Transfer Conf. Digital Library (1986) 2343–2348.
[41] W. Lu, Forced convective boiling in liquid nitrogen from discrete heat sources Ph.D. Thesis, University of Kentucky, 1998.
[42] A.V. Klimenko, A.M. Sudarchikov, V.V. Klimenko, Boiling crisis of nitrogen in a channel at low flow rates and high pressures, Heat Transfer Research 32 (2001) 130–135.
[43] A.V. Klimenko, A.M. Sudarchikov, Investigation of hydrodynamic instability at a forced flow boiling of nitrogen in a channel at high pressures, Int. Heat Transfer Conf. Digital Library (2002).
[44] S.L. Qi, P. Zhang, R.Z. Wang, L.X. Xu, Flow boiling of liquid nitrogen in micro-tubes: Part I–The onset of nucleate boiling, two-phase flow instability and two-phase flow pressure drop, Int. J. Heat Mass Transfer 50 (2007) 4999–5016.
[45] S.L. Qi, P. Zhang, R.Z. Wang, L.X. Xu, Flow boiling of liquid nitrogen in micro–tubes: Part II–Heat transfer characteristics and critical heat flux, Int. J. Heat Mass Transfer 50 (2007) 5017–5030.
[46] A. Trejo, A. Trujillo, M. Galvan, A. Choudhuri, J.C. Melcher, J.J. Bruggemann, Experimental investigation of methane convection and boiling in rocket engine cooling channels, Journal of Thermophysics and Heat Transfer 30 (2016) 937–945.
[47] S. Mustafi, High Reynolds number vertical up-flow parameters for cryogenic two-phase helium I Ph.D. Thesis, University of Maryland, 2014.
[48] M. Shiotsu, Y. Shirai, Y. Oura, Y. Horie, K. Yoneda, H. Tatsumoto, K. Hata, H. Kobayashi, Y. Naruo, Y. Inatani, Film boiling heat transfer from a round wire to liquid hydrogen flowing upward in a concentric annulus, Physics Procedia 67 (2015) 631–636.
[49] H. Tatsumoto, Y. Shirai, M. Shiotsu, Y. Naruo, H. Kobayashi, Y. Inatani, Transient heat transfer from a wire inserted into a vertically mounted pipe to forced flow liquid hydrogen, Physics Procedia 67 (2015) 649–654.
[50] K. Yoneda, Y. Shirai, M. Shiotsu, Y. Oura, Y. Horie, T. Matsuzawa, H. Shigeta, H. Tatsumoto, K. Hata, Y. Naruo, H. Kobayashi, Y. Inatani, Forced flow boiling heat transfer properties of liquid hydrogen for manganin plate pasted on one side of a rectangular duct, Physics Procedia 67 (2015) 637–642.
[51] T. Matsumoto, Y. Shirai, M. Shiotsu, K. Fujita, T. Kainuma, H. Tatsumoto, Y. Naruo, H. Kobayashi, S. Nonaka, Y. Inatani, DNB heat flux in forced convection of liquid hydrogen for a wire set in central axis of vertically mounted flow channel, In IOP Conf. Ser.: Mater. Sci. Eng. 278 (2017) 012034.
[52] Y. Shirai, T. Kainuma, H. Shigeta, M. Shiotsu, H. Tatsumoto, Y. Naruo, H. Kobayashi, S. Nonaka, Y. Inatani, S. Yoshinaga, Liquid hydrogen recirculation system for forced flow cooling test of superconducting conductors, In IOP Conf. Ser.: Mater. Sci. Eng. 278 (2017) 012036.
[53] T. An, Y. Wang, W.Q. Liu, Experimental investigation of heat transfer characteristics of liquid nitrogen flow boiling in a mini-channel, Int. Heat Transfer Conf. Digital Library (2018) 6479–6485.
[54] V.A. Grigor'ev, V.I. Antipov, Y.M. Pavlov, A.V. Klimenko, Experimental investigation of heat transfer with boiling of nitrogen and helium in tubes, Teploenergetika 24 (1978) 12–15.
[55] J.P. Lewis, J.H. Goodykoontz, J.F. Kline, Boiling heat transfer to liquid hydrogen and nitrogen in forced flow. National Aeronautics and Space Administration Technical Note D-1314, 1962.
[56] G. Hildebrandt, Heat transfer to boiling helium-I under forced flow in a vertical tube, in: Proc. 4th Int. Cryo. Eng. Conf., 1972, pp. 295–300.
[57] H. Ogata, S. Sato, Critical heat flux for two-phase flow of helium I, Cryogenics 13 (1973) 610–611.
[58] H. Ogata, S. Sato, Forced convection heat transfer to boiling helium in a tube, Cryogenics 14 (1974) 375–380.
[59] B.S. Petukhov, V.M. Zhukov, V.M. Shieldcret, Investigation of heat transfer and hydrodynamics in the helium two-phase flow in a vertical channel, In Advanced Course in Heat Exchangers: Theory and Practice, ICHMT Symposium (1981) 251–262.
[60] B.S. Petukhov, V.M. Zhukov, S.B. Anisimov, Cryogenic liquids forced boiling heat transfer in a rotating channel, Cryogenics 26 (1986) 226–233.
[61] R. Yun, J.S. Hwang, J.T. Chung, Y. Kim, Flow boiling heat transfer characteristics of nitrogen in plain and wire coil inserted tubes, Int. J. Heat Mass Transfer 50 (2007) 2339–2345.
[62] P. Zhang, X. Fu, Two-phase flow characteristics of liquid nitrogen in vertically upward 0.5 and 1.0 mm micro-tubes: visualization studies, Cryogenics 49 (2009) 565–575.
[63] B. Zhang, Q. Li, Y. Wang, J. Zhang, P. Zhang, H. Jia, Experimental investigation of flow boiling heat transfer boundary of nitrogen in 1.2 mm vertical mini-channel, Int. Heat Transfer Conf. Digital Library (2018) 6861–6868.
[64] B.C. Zhang, Q.L. Li, Y. Wang, J.Q. Zhang, J. Song, F.C. Zhuang, Experimental investigation of nitrogen flow boiling heat transfer in a single mini-channel, Journal of Zhejiang University-SCIENCE A 21 (2020) 147–166.
[65] Y. Shirai, H. Tatsumoto, M. Shiotsu, K. Hata, H. Kobayashi, Y. Naruo, Y. Inatani, DNB heat flux on inner side of a vertical pipe in forced flow of liquid hydrogen and liquid nitrogen, Cryogenics 92 (2018) 105–117.
[66] C.C. Wright, H.H. Walters, Single tube heat transfer tests—Gaseous and liquid hydrogen, Wright Air Development Center Technical Report 59-423, 1959.
[67] D. Steiner, E.U. Schlünder, Heat transfer and pressure drop for boiling nitrogen flowing in a horizontal tube: 1. Saturated flow boiling, Cryogenics 16 (1976) 387–398.
[68] V.P. Beliakov, V.A. Shaposhnikov, S.P. Gorbatchev, I.I. Michailov, E.D. Mikitenko, Studies on nucleate boiling crisis of helium-I in channels of superconducting magnet systems, IEEE Transactions on Magnetics 15 (1979) 40–45.
[69] V.I. Romanov, A.L. Sevryugin, Yu.M. Pavlov, V.I. Antipov, Investigating burnouts with helium boiling in a channel, Teploenergetika 28 (1981) 620–622.
[70] I.L. Yarmak, V.M. Zhukov, Forced liquid helium flow transient heat transfer in a narrow channel under step heat flux, Cryogenics 32 (1992) 729–736.
[71] U.H. von Glahn, J.P. Lewis, Nucleate-and film-boiling studies with liquid hydrogen, Adv. Cryog. Eng. 5 (1960) 262–269.
[72] H. Tatsumoto, Y. Shirai, M. Shiotsu, K. Hata, H. Kobayashi, Y. Naruo, Y. Inatani, T. Kato, K. Kinoshita, Forced convection heat transfer of subcooled liquid hydrogen in a small tube, in: Proc. of ICEC23-ICMC, 2010, pp. 491–496.
[73] Y. Shirai, H. Tatsumoto, K. Hata, M. Shiotsu, H. Kobayashi, Y. Naruo, Y. Inatani, Preliminary study on heat transfer characteristics of liquid hydrogen for coolant of HTC superconductors, In AIP Conference Proceedings 1218 (2010) 337–339.
[74] H. Tatsumoto, Y. Shirai, M. Shiotsu, K. Hata, H. Kobayashi, Y. Naruo, Y. Inatani, T. Kato, M. Futakawa, K. Kinoshita, Development of a thermal-hydraulics experimental system for high Tc superconductors cooled by liquid hydrogen, In J. Phys.: Conf. Ser 234 (2010) 032056.
[75] Y. Shirai, H. Tatsumoto, M. Shiotsu, K. Hata, H. Kobayashi, Y. Naruo, Y. Inatani, K. Kinoshita, Forced flow boiling heat transfer of liquid hydrogen for superconductor cooling, Cryogenics 51 (2011) 295–299.
[76] Y. Shirai, M. Shiotsu, H. Kobayashi, T. Takegami, H. Tatsumoto, K. Hata, H. Kobayashi, Y. Naruo, Y. Inatani, K. Kinoshita, DNB heat flux in forced flow of subcooled liquid hydrogen under pressures, In AIP Conference Proceedings 1434 (2012) 1067–1074.
[77] H. Tatsumoto, Y. Shirai, M. Shiotsu, K. Hata, Y. Naruo, H. Kobayashi, Y. Inatani, K. Kinoshita, Forced convection heat transfer of liquid hydrogen through a 200-mm long heated tube, Physics Procedia 36 (2012) 1360–1365.
[78] H. Tatsumoto, Y. Shirai, M. Shiotsu, K. Hata, Y. Naruo, H. Kobayasi, Y. Inatani, Forced convection heat transfer of saturated liquid hydrogen in vertically–mounted heated pipes, In AIP Conference Proceedings 1573 (2014) 44–51.
[79] T. Matsumoto, Y. Shirai, M. Shiotsu, K. Fujita, Y. Iwami, Y. Naruo, H. Kobayashi, S. Nonaka, Y. Inatani, Film boiling heat transfer properties of liquid hydrogen flowing inside of heated pipe, In IOP Conference Series: Materials Science and Engineering 502 (2019) 012090.
[80] H. Tatsumoto, Y. Shirai, M. Shiotsu, K. Hata, Y. Naruo, H. Kobayashi, Y. Inatani, K. Kinoshita, Forced convection heat transfer of subcooled liquid hydrogen in horizontal tubes, In AIP Conference Proceedings 1434 (2012) 747–754.
[81] C. Johannes, Recent advances in heat transfer to helium 1, Revue de Physique Appliquée 6 (1971) 509–513.
[82] V.E. Keilin, I.A. Kovalev, V.V. Likov, M.M. Pozvonkov, Forced convection heat transfer to liquid helium I in the nucleate boiling region, Cryogenics 15 (1975) 141–145.
[83] V.V. Arkhipov, S.V. Kvasnyuk, V.I. Deev, V.K. Andreev, An experimental investigation and method of calculation of critical heat loads when boiling helium in tubes, Teploenergetika 26 (1979) 27–29.
[84] V.I. Deev, V.I. Petrovichev, A.I. Pridantsev, Yu.V. Gordeev, V.V. Arkhipov, V.V. Parygin, Hydraulic resistance and burnout with helium boiling in tubes, Teploenergetika 26 (1979) 45–47.
[85] V.I. Subbotin, V.I. Deev, V.V. Arkhipov, Critical heat flux in flow boiling of helium, Int. Heat Transfer Conf. Digital Library (1982) 357–361.
[86] Y. Katto, S. Yokoya, Critical heat flux of liquid helium (I) in forced convective boiling, Int. J. Multiphase Flow 10 (1984) 401–413.
[87] V.I. Subbotin, V.I. Deev, A.I. Pridantsev, V.K. Andreev, V.V. Arkhipov, V.N. Novikov, A.N. Savin, V.V. Solodovnikov, Heat transfer and hydrodynamics in cooling channels of superconducting devices, Cryogenics 25 (1985) 261–265.
[88] P. Bredy, D. Neuveglise, M.X. Francois, C. Meuris, R. Duthil, Test facility for helium I two phase flow study, Cryogenics 34 (1994) 361–364.
[89] P.J. Giarratano, R.C. Hess, M. C. Jones, Forced convection heat transfer to subcritical helium I, National Bureau of Standards Report 73-322, 1973.
[90] P.J. Giarratano, R.C. Hess, M.C. Jones, Forced convection heat transfer to subcritical helium I, Adv. Cryog. Eng. 19 (1995) 404–416.
[91] S.S. Papell, R.J. Simonaeu, D.D. Brown,. Buoyancy effects on critical heat flux of forced convective boiling in vertical flow, National Aeronautics and Space Administration Technical Note D-3672, 1966.
[92] H. Tatsumoto, Y. Shirai, K. Hata, T. Kato, M. Futakawa, M. Shiotsu, Forced convection heat transfer of subcooled liquid nitrogen in a vertical tube, In Journal of Physics: Conference Series 234 (2010) 032057.

[93] H.M. Muller, W. Bonn, D. Steiner, Heat transfer and critical heat flux at flow boiling of nitrogen and argon within a horizontal tube, In Advanced Course in Heat Exchangers: Theory and Practice. ICHMT Symposium (1981) 233–250.
[94] H. Tatsumoto, Y. Shirai, K. Hata, T. Kato, M. Shiotsu, Forced convection heat transfer of subcooled liquid nitrogen in horizontal tube, In AIP Conference Proceedings 985 (2008) 665–672.
[95] X. Liu, X. Chen, Q. Zhang, S. Wang, Y. Hou, L. Chen, Investigation on CHF of saturated liquid nitrogen flow boiling in a horizontal small channel, Appl. Therm. Eng. 125 (2017) 1025–1036.
[96] M.R. Glickstein, R.H. Whitesides, Forced-convection nucleate and film boiling of several aliphatic hydrocarbons, In ASME-AIChE Heat Transfer Conference and Exhibit 67-HT-7 (1967) 1–8.
[97] J. Van Noord, A heat transfer investigation of liquid and two-phase methane, National Aeronautics and Space Administration Technical Memorandum 2010-216918 (2010).
[98] Y. Katto, S. Yokoya, Critical heat flux of forced convective boiling in uniformly heated vertical tubes with special reference to very large length-to-diameter ratios, Int. J. Heat Mass Transfer 30 (1987) 2261–2269.
[99] C.F. Coolebrook, Turbulent flow in pipes with particular reference to the transition region between the smooth and rough pipes laws, J. Inst. Civ. Eng. 11 (1939) 133–156.
[100] S.M. Zivi, Estimation of steady-state steam void-fraction by means of the principle of minimum entropy production, ASME J. Heat Transfer 86 (1964) 247–252.
[101] D.D. Hall, I. Mudawar, Ultra-high critical heat flux (CHF) for subcooled water flow boiling – II: high-CHF database and design equations, Int. J. Heat Mass Transfer 42 (1999) 1429–1456.
[102] MATLAB Global Optimization Toolbox, R2018b, Version 9.5.0.944444: The MathWorks Inc., Natick, MA, 2018.
[103] M. Shah, Improved general correlation for critical heat flux during upflow in uniformly heated vertical tubes, Int. J. Heat Fluid Flow 8 (1987) 326–335.